Nucleic Acids Research, 2024, 1–20
https://doi.org/10.1093/nar/gkae507
Molecular Biology

Zika virus non-coding RNAs antagonize antiviral responses by PKR-mediated translational arrest

Horacio M. Pallarés[1], María Mora González López Ledesma[1], Santiago Oviedo-Rouco[1], Luciana A. Castellano[2], Guadalupe S. Costa Navarro[1], Ana J. Fernández-Alvarez[1], María Josefina D'Andreiz[1], Victor Daniel Aldas-Bulos[2], Diego E. Alvarez[3], Ariel A. Bazzini[2,4] and Andrea V. Gamarnik[1,*]

[1]Fundación Instituto Leloir, Instituto de Investigaciones Bioquímicas de Buenos Aires IIBBA-CONICET, Ciudad Autónoma de Buenos Aires, Argentina
[2]Stowers Institute for Medical Research, Kansas City, MO, USA
[3]Instituto de Investigaciones Biotecnológicas, Universidad Nacional de San Martín-CONICET, Buenos Aires, Argentina
[4]Department of Molecular and Integrative Physiology, University of Kansas Medical Center, 3901 Rainbow Blvd, Kansas City, KS 66160, USA
[*]To whom correspondence should be addressed. Tel: +54112387500; Fax: +54112387501; Email: agamarnik@leloir.org.ar

Abstract

Zika virus (ZIKV) is an emerging mosquito-borne flavivirus that causes severe outbreaks in human populations. ZIKV infection leads to the accumulation of small non-coding viral RNAs (known as sfRNAs) that are crucial for evasion of antiviral responses and for viral pathogenesis. However, the mechanistic understanding of how sfRNAs function remains incomplete. Here, we use recombinant ZIKVs and ribosome profiling of infected human cells to show that sfRNAs block translation of antiviral genes. Mechanistically, we demonstrate that specific RNA structures present in sfRNAs trigger PKR activation, which instead of limiting viral replication, enhances viral particle production. Although ZIKV infection induces mRNA expression of antiviral genes, translation efficiency of type I interferon and interferon stimulated genes were significantly downregulated by PKR activation. Our results reveal a novel viral adaptation mechanism mediated by sfRNAs, where ZIKV increases its fitness by repurposing the antiviral role of PKR into a proviral factor.

Graphical abstract

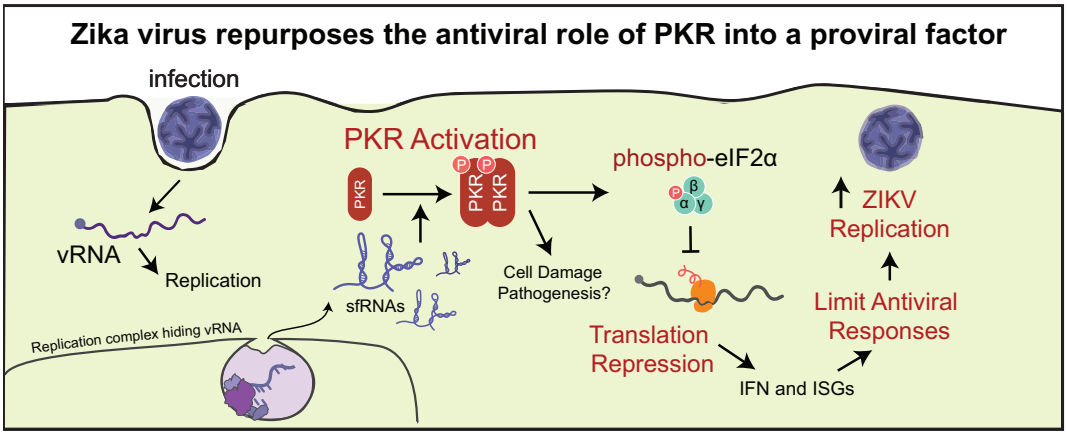

Introduction

Flaviviruses are emerging and reemerging RNA viruses that include important human pathogens, such as Zika (ZIKV), dengue (DENV), yellow fever, West Nile and Japanese encephalitis viruses. The genome of flaviviruses is a single molecule that contains conserved RNA structures that modulate viral replication and counteract antiviral responses (1,2). The viral 3′ untranslated region (UTR) contains duplications of RNA elements that fold into unique structures that halt 5′ to 3′ degradation of the genome, leading to the accumulation of viral non-coding RNAs, known as sfRNAs. Information from different laboratories support a crucial role of

Received: January 18, 2024. **Revised:** May 8, 2024. **Editorial Decision:** May 29, 2024. **Accepted:** June 4, 2024

sfRNAs in evasion of innate antiviral responses and in viral pathogenesis (3–8). While there is consensus on the relevance of sfRNAs, the molecular understanding of how they function is still unclear. In this study, we use ZIKV to dissect the mechanism by which sfRNAs interfere with the human cell translation machinery to control innate immune responses.

ZIKV is an emerging virus responsible for severe outbreaks in human populations. In 2015–2017, an explosive epidemic of ZIKV took place in South and Central America. Unique properties of ZIKV infection, related to sexual transmission and dissemination through the placenta, pose important challenges to the healthcare system. Although about 80% of infections were asymptomatic or mild, the virus caused neurological disorders in adults, such as Guillain-Barré syndrome. Moreover, infections during pregnancy led to severe congenital neurological abnormalities, known as congenital Zika syndrome (CZS). The most well-known feature of CZS is microcephaly, but the syndrome also includes general neurological impairment, neurosensory alterations, delays in motor development, and high risk of death during the first three years of life. The devastating impact of ZIKV on newborns, coupled with its potential for sexual transmission, caused profound social consequences, placing women in vulnerable positions in many countries of Latin America. Albeit the global impact of ZIKV, still there are no effective countermeasures for controlling or preventing infections with this pathogen.

ZIKV infection mainly results in the accumulation of two species of sfRNAs. These RNAs are the products of halting genome degradation by the host XRN1 enzyme in two RNA structures of the ZIKV 3′UTR, known as xrRNA1 and xrRNA2 (9). We have recently shown that these RNA structures play host-specific functions in human cells and in *Aedes aegypti* mosquitoes, and found that they work in a cooperative manner to produce sfRNAs during ZIKV infection (10). In addition, it has been recently reported that ZIKV sfRNAs interact with the viral protein NS5, increasing its stability, reducing STAT1 phosphorylation and limiting IFN signaling (11). Using human brain organoids, the same study associated the accumulation of sfRNAs with ZIKV-induced death of neural progenitor cells, providing further evidence for the role of these RNAs in viral pathogenesis. It is important to highlight that distinct flaviviruses produce different types of sfRNAs with varying lengths and cellular levels during infection (8,12–16). It is likely that selective pressure during virus evolution led to fine tune the quality of sfRNAs produced by each virus depending on the antiviral responses in distinct host species, viral tropism, and viral replication requirements. Different roles have been assigned to sfRNAs during infection in human and mosquito hosts (6,17–20). In DENV, it has been proposed that sfRNAs act as sponges, sequestering RNA-binding proteins that are involved in antiviral responses, dysregulating cellular mRNA decay, and modulating host RNA splicing (21–24). Moreover, accumulation of different amounts of sfRNAs during infection has been linked with distinct epidemiological fitness of DENV isolates (24), indicating the relevance and complexity of sfRNA functions in flavivirus infections.

In this study, we examine the impact of sfRNA accumulation on the host machinery during ZIKV infection. Using ribosome profiling of human cells infected with viruses that either can or cannot generate sfRNAs, we found that sfRNA accumulation is responsible for translation repression mediated by PKR activation. PKR is an antiviral kinase induced by type I interferon (IFN) that senses double-stranded RNA (dsRNA) intermediates of viral replication. PKR is activated by dsRNA, leading to phosphorylation of the α subunit of the translation initiation factor 2 (eIF2α) inhibiting translation initiation as a strategy to limit viral protein synthesis (25,26). Our data show that ZIKV sfRNAs promote PKR auto-phosphorylation, which, instead of inhibiting viral processes, increases ZIKV replication and enhances secretion of infectious particles. In this regard, limiting sfRNA production or downregulating PKR, enhances type I IFN protein synthesis and increases the accumulation of interferon-stimulated genes (ISG) proteins. The data support a model in which sfRNAs induce PKR phosphorylation to inhibit translation of antiviral genes. We conclude that ZIKV has evolved a mechanism to repurpose an antiviral pathway into a proviral process. In addition, because PKR activation is associated with cell damage and neurological abnormalities, the link between sfRNA accumulation and PKR activation may be relevant for understanding ZIKV pathogenesis.

Materials and methods

Viral isolate

We used an epidemic ZIKV infectious clone, originated from a clinical isolate obtained in Argentina in 2016 (ARCB116141, GenBank MK637519.2) (10,27).

RNA transcription, transfection and viral infection

A plasmid containing the full-length sequence of the epidemic isolates (**pZIKVAr**) was linearized with KpnI and used for *in vitro* transcription using T7 RNA polymerase (Ambion) in the presence of m7GpppA cap analog (NEB). RNA quantification was assessed using a Qubit4 (Invitrogen), and RNA integrity was confirmed through electrophoresis on 1% agarose gels. RNA transcripts were transfected into C6/36HT and A549 cells using Lipofectamine 2000 and Opti-MEM media (Invitrogen). Viruses were harvested at specific time intervals. To generate viral stocks, C6/36HT cells were used.

Cells culture

ZIKV infections were conducted using the following cell lines. C6/36HT cells (CVCL_VH42), an *Aedes albopictus* cell line adapted for growth at 33°C (28), were cultured in Leibovitz's L-15 medium supplemented with 10% fetal bovine serum, 100 U/ml penicillin, 100 μg/ml streptomycin, 0.3% tryptose phosphate broth, 0.02% glutamine, 1% minimal essential medium (MEM) nonessential amino acids solution, and 0.25 μg/ml amphotericin B (Fungizone). A549 WT and PKR-/- cells (human epithelial lung cell line) were cultured in Dulbecco's modified Eagle's medium with nutrient mixture F-12 (DMEM/F-12) supplemented with 10% fetal bovine serum, 100 U/ml penicillin, and 100 μg/ml streptomycin. A549 PKR-/- knock out (PKR KO) cell line was provided by Dr. Susan Weiss (29). Huh-7 cells (human hepatocyte cell line) and HEK-293T cells (human embryonic kidney cell line) were cultured in Dulbecco's modified Eagle's high-glucose medium (4500 mg/liter) supplemented with 10% fetal bovine serum, 100 U/ml penicillin, and 100 μg/ml streptomycin.

Recombinant ZIKVs

Mutations were introduced into the full-length cDNA of ZIKV ARCB116141 pZIKVAr by replacing the

AgeI-KpnI fragment with the respective fragment derived from overlapping PCRs containing the desired mutations. This was achieved using the oligonucleotides described in Supplementary Table S1. Deletions were designed as follows: ZIKVΔxrRNA1 lacked nucleotides 10 399 to 10 466, ZIKVΔxrRNA2 lacked nucleotides 10 482 to 10 547, and ZIKVsfRNAnull lacked nucleotides 10 399 to 10547.

Viral titration

Viral titers were determined by fluorescent-based focus forming units (FFU) in C6/36HT cells. Cells were prepared in 24-well plates and infected with serial ten-fold dilutions, then covered with semi-solid L-15 medium containing 0.8% carboxymethyl cellulose (Sigma-Aldrich). After incubation at 33°C for 9 days, the medium was removed, cells were fixed with 4% paraformaldehyde in PBS with sucrose for 20 minutes at room temperature, and then blocked in 250 µl/well of B buffer (2.5% Bovine Serum, Internegocios; 0.1% Tween 20-PBS) at room temperature for 1 h. The blocking buffer was then replaced with 250 µl/well of rabbit polyclonal anti-NS3 antibody (1:500 in blocking buffer) for 1 h at room temperature. After washing three times with 0.1% Tween 20–PBS, the cells were subjected to Alexa Fluor™ 488-conjugated goat anti-rabbit IgG (Thermofisher, 1:500 in blocking buffer) for 1 hour. Finally, the cells were washed three times with 0.1% Tween 20-PBS and 500 µl of PBS was added to each well. The foci forming units were counted in the Zeiss Axio Observer 3 inverted fluorescence microscope.

RNA quantification

For qRT-PCR of viral RNA, total RNA samples were used for reverse transcription as previously described (10). Reactions were performed in duplicates in 96-well plates using 2 µl of the RT reaction mixture as the template, 5 µl of FastStart SYBR Green Master 2 × mix (Roche), 300 nM of each primer, and RNase-free water to a total volume of 10 µl. The primers AVG2098 (5′- GCCGCCACCAAGATGAACTGATTG-3′) and AVG2099 (5′-GCAGTCTCCCGGATGCTCCATC-3′) were targeted to amplify nucleotides 9937 to 10 113 within the NS5 coding sequence. For quantification of IFNβ, ISGs, and ISR genes, qRT-PCR was used, and the oligonucleotides employed are detailed in Supplementary Table S1.

Antibodies and immunofluorescence assays

For immunofluorescence and Western blot assays the following antibodies were used mouse monoclonal anti-PKR (Santa Cruz, sc-100378), rabbit monoclonal anti-phosphoPKR (ABCAM ab32036), mouse monoclonal anti-eIF2α (Cell Signaling L57A5), rabbit monoclonal anti-phospho-eIF2α (Cell Signaling #9721), rabbit monoclonal anti-G3BP1 (BD Transduction Laboratories #611 126), goat polyclonal anti-eIF3η (Santa Cruz, sc-16377), mouse monoclonal anti-TIAR (BD Transduction Laboratories #610 352), rabbit monoclonal anti-OAS3 (ABCAM ab154270), rabbit monoclonal anti-TRIM5α (Cell Signaling, D6Z8L), mouse monoclonal anti-GAPDH (ABCAM ab9245) and rabbit monoclonal anti-PERK (Cell Signaling, C33E10). For detection of ZIKV antigens, rabbit polyclonal anti-NS3, anti-NS5 obtained in our laboratory and mouse monoclonal anti-E (E18, kindly provided by the Department of Molecular Microbiology laboratory, Washington University School of Medicine) were used. Immunofluorescence assays (IFA) were performed as followed: Human A549 cells infected with WT or recombinant ZIKV were grown in 24-well plates containing 1-cm^2 coverslips. At various times post-infection, coverslips were removed, and cells were fixed with paraformaldehyde 4%, sucrose 4%, in PBS pH 7.4 at room temperature for 20 minutes. Alternatively, cells were fixed with methanol for 20 min at −20°C. PFA fixed cells were then permeated with 0.1% Triton X-100 for 4 min at room temperature. Images were obtained with a Zeiss LSM 880 Airyscan confocal microscope.

Knock-down assays

RNA interference experiments followed the procedure previously described (30) and employed ON-TARGET plus SMART pool siRNA oligonucleotides from Dharmacon RNA Technologies in Lafayette, CO, USA. A non-related siRNA (siRNA NR, Dharmacon) served as a negative control. A549 cells were transfected with the corresponding siRNA using Oligofectamine (Invitrogen). After 48 h of transfection, cells were infected with ZIKV at different moi.

Cell viability

The viability of A549 cells following transfection with non-related (nr) and PKR siRNA was determined by measuring cellular ATP levels, indicative of metabolic activity at different hpt. This was achieved using the CellTiter-Glo® Luminescent Cell Viability Assay kit (Promega), following the manufacturer's instructions.

ELISA assays

Human IFN-β was procured from pbl assay science (41410-1), and the cytokine levels were measured in the cell supernatant following the manufacturer's instructions.

In vitro sfRNAs production

Firstly, PCRs were generated using pZIKVAr as a template and used for *in vitro* transcription with T7 RNA polymerase from Ambion. RNA quantification was assessed using a Qubit4 (Invitrogen), and RNA integrity was confirmed on 1% agarose gels. RNA transcripts were treated with DNAseI (Roche), purified with LiCl 7.5 M precipitation, and then 1.5 ug of RNA was treated with RNA Pyrophosphohydrolase (NEB, M0356S) following the manufacturer's instructions. Each RNA was transfected into A549 cells at a concentration of 400 ng/ml using Lipofectamine 2000 (Invitrogen), and cell extracts were harvested at different hours post-transfection for western Blot analysis. The RNAs were designed as follows: sfRNA1 from nucleotide 10 393 to 10 807, sfRNA2 from nucleotide 10 477 to 10 807, ΔxrRNA1/2 from nucleotide 10 358 to 1087 with a deletion from nucleotide 10 393 to 10 542, ΔpDB from nucleotide 10 393 to 1087 with a deletion from nucleotide 10 559 to 10 609, ΔDB from nucleotide 10 393 to 1087 with a deletion from nucleotide 10 613 to 10 685, and Δ3'SL from nucleotide 10 393 to 10710.

XRN1 *in vitro* assay

450 ng of each 5′p-RNA was incubated for an hour at 37°C with recombinant XRN1 (NEB, M0338L) and then heat inactivated at 70°C for 10 min. RNA integrity was assessed with an electrophoretic run on a 2% agarose gel.

Northern blot assay

For ZIKV sfRNA detection, total RNA was obtained using TRIzol from infected cells and separated on 5% polyacrylamide 7 M urea gels. RNA was then transferred onto a nylon membrane (Hybond-N; GE Healthcare) using a semidry blotting apparatus and UV cross-linked. For the detection of genomic RNA (gRNA), samples were loaded into a slot blot apparatus using nylon membranes (Hybond-N; GE Healthcare). The membranes were blocked overnight (ON) at 68°C in DIG Easy Hyb granule (Sigma-Aldrich) hybridization solution. Uniformly digoxigenin-labeled RNA probes were obtained by *in vitro* transcription using the DIG Northern starter kit (Sigma-Aldrich). Two RNA probes were designed: one for detecting genomic RNA that hybridizes with the 5´UTR, and the other for detecting both genomic RNA and sfRNAs that hybridizes with the 3´UTR. The 5´ probe was complementary to nucleotides 1–483 of the viral genome, and the 3´ probe was complementary to the complete 3´UTR (nucleotides 10 373–10 807). Northern blots were visualized with the ImageQuant LAS 4000 (GE Healthcare Life Sciences).

ISRIB inhibition assay

A549 cells were infected with ZIKV for two hours, followed by treatment with 25, 100 and 400 nM of ISRIB (Sigma Aldrich, SML0843). Cells were then harvested at 12 and 24 h post-infection and the viral replication was assessed by RT-qPCR.

Ribosome profiling

The ribosome profiling protocol followed previous procedures (31). In brief, ribosome protected fragments were collected from duplicate samples of A549 cells infected with ZIKV wild type or sfRNAnull mutant at 20 hpi. A p100 dish of A549 cells was incubated with cycloheximide (0.1 μg/ml) in PBS for 5 minutes. The PBS was removed, and the cells were treated with Lysis buffer (20 mM total Tris–HCl pH 8.0; 140 mM KCl; 1.5 mM $MgCl_2$; 100 μg/ml cycloheximide; 1% Triton; 40 U/ml SUPERas In (Ambion #AM2694); 10 μl/ml protease inhibitor cocktail (Calbiochem #535140-1ML)). The mix was clarified for 10 min at 10 000g at 4°C. RNase I (100 units, Ambion #AM2295) and DNase (10 units, Ambion #AM2238) were added to the supernatant and incubated at room temperature for 45 min with gentle mixing. Digested extracts (50 μl) were then overlaid onto s-40 columns following the manufacturer's instructions. RNA was extracted using Trizol (Invitrogen, #800 868)

RNA input

RNA for each sample was collected in parallel with the ribosome profile experiment for RNA preparation. RNA was extracted using Trizol (Invitrogen, #800 868).

Small RNA sequencing libraries

Ribosome protected fragments (RPF) were separately excised in a 15% urea gel from 28-to-38 nucleotides. RNA was eluted overnight in 300 mM NaOAc pH 5.5; 1 mM EDTA; 0.1 U/μl SUPERas In (Ambion #AM2694), followed by ethanol precipitation. RFP were 3′-dephosphorylated with polynucleotide kinase (10 U, PNK, New England Biolabs) in T4 polynucleotide kinase buffer (without ATP) for 1 h at 37°C, followed by a 10 min incubation at 75°C and ethanol precipitation. All RNA samples were resuspended and ligated to 3′ adaptor (30 μM /5rApp/ATCTCGTATGCCGTCTTCTGCTTG/3ddC/) using T4 RNA Ligase 2, truncated K227Q (2 U, New England Biolabs; #M0351S) and RNAseOUT Recombinant Ribonuclease Inhibitor (5 U, Invitrogen, #10777-019) for 6 h at 20°C. Ligation reactions were separately in a 10% urea gel, and fragments from 50-to-65 nucleotides for the RPF and 50-to-75 nucleotides were excised, eluted, and precipitated from the gel. The 3′-ligation products were then 5′-phosphorylated with polynucleotide kinase (15 U, PNK, New England Biolabs) in T4 polynucleotide kinase buffer supplemented with 1 mM ATP for 30 min at 37°C followed by RNA precipitation in ethanol. The 5′-ligation was performed using T4 RNA Ligase 1 (ssRNA Ligase, 10 U New England Biolabs, #M0204S) for 6 h at 20°C with barcoded 5´-Adaptor (100 μM, GUUCAGAGUUCUACAGUCCGACGAUCAAAC; GUUCAGAGUUCUACAGUCCGACGAUCGGGC; GUUCAGAGUUCUACAGUCCGACGAUCUUUC; GUUCAGAGUUCUACAGUCCGACGAUCCCCC; GUUCAGAGUUCUACAGUCCGACGAUCACUC; GUUCAGAGUUCUACAGUCCGACGAUCGACC; GUUCAGAGUUCUACAGUCCGACGAUCUGAC; GUUCAGAGUUCUACAGUCCGACGAUCCUGC). The 5′-ligation reactions were separately in a 10% urea gel, and the region from 80-to-95 nucleotides for the RPFs and 80-to-105 nucleotides for the RNA input samples was excised, eluted, and precipitated from the gel. Gel-purified samples were reverse transcribed using SuperScript™ II Reverse Transcriptase (Invitrogen) with RTOligo (CAAGCAGAAGACGGCATACGA) according to the manufacturer (Invitrogen). Amplification was done using Phusion High-Fidelity DNA Polymerase (Thermo Scientific) and oligos: AATGATACGGCGACCACCGACAGGTTCAGAGTTCTACAGTCCGA and CAAGCAGAAGACGGCATACGA. PCR was carried out with an initial 30 s denaturation at 98°C, followed by 4 cycles of 30 s denaturation at 98°C, and 15 s extension at 72°C. Followed by 10–15 cycles of 10 s denaturation at 98°C, 30 s annealing at 50°C, and 15 s extension at 72°C. Several reactions, with different numbers of cycles, were performed. Reactions were separated on a non-denaturing 8% polyacrylamide TBE gel, and DNA fragments of the correct size were extracted and sequenced using Illumina HiSeq2000.

Sequencing data processing

Raw RNA-seq reads were demultiplexed into Fastq format, with a tolerance of one mismatch, using Illumina bcl-convert version 3.10.5. Subsequently, the reads were mapped to the UCSC genome hg38 using the STAR aligner version 2.7.3a (Ensembl 102 gene models were employed for this alignment). Ribosome profiling data was processed using the Riboseeker R package. Ribo-seq reads were first filtered by read length to keep only the read lengths between 20 and 40 nt, mapping them to a set of non-coding RNAs using bowtie2 version 2.4.2. Unmapped reads were then aligned to the reference genome (hg38) and ZIKV genome (MT636065) using STAR. Genomic features were calculated using Picard tools version 2.25.7. Only 28–32 bp long reads were used for downstream analysis.

Metagene plot

These plots were made in R using the RiboSeeker package (https://github.com/nzhang89/RiboSeeker). First, for each

gene, we only kept its longest transcript. Then, the top 2000 transcripts with the highest estimated RPKMs were selected, with a requirement that these transcripts met specific criteria, including a CDS, 5′-UTR, and 3′-UTR length of 50 bp or more. The estimation of RPKM involved several steps: firstly, only the 5′-most position of each mapped read was kept; then, the 5′- and 3′-positions of each transcript were shifted by −12 bp, respectively, and the first and last 6 bp were excluded from each transcript after shifting. Two windows with a length of 100 bp each were chosen around the coding start and coding end positions for each of the 2000 selected transcripts. In the next phase, read counts were normalized (with reads resized to the 5′-most positions) for each position within these two specified windows to the total number of reads within those windows for each selected transcript.

Sequencing data analysis

Downstream analyses were performed on R 4.2.3. Principal Components Analysis and Pearson correlation matrix were plotted using ggplot version 3.4.3. Differential gene expression analysis was conducted using edgeR version 3.40.2, lowly expressed genes were filtered out using the filterByExpr function. Translation efficiency was calculated for all the retained genes as $\log_2$((rpkm of RPF + 0.00001)/(rpkm of RNA level + 0.00001)) of the CDS, excluding the start and stop codon. Control groups were generated using clustering k-nearest neighbor's algorithm to find a set of genes with the closest RNA expression level distribution to the group of genes of interest.

Statistical analysis

All statistical tests and plots were conducted using GraphPad Prism 8.0 software. *P*-values were calculated using the Mann–Whitney *U* test to compare the mean values of two groups. Statistical significance is indicated in the figure legends with the following notations: $*P < 0.05$; $**P < 0.01$; $***P < 0.001$; ns (non-significant).

Results

Accumulation of ZIKV sfRNAs reduce type I IFN protein production

To investigate the mechanism underlying the function of sfRNAs during ZIKV infection, we designed viruses impaired in sfRNA production. ZIKV relies mainly on two RNA structures in the 3′UTR (xrRNA1 and xrRNA2) for sfRNA1 and sfRNA2 generation (Figure 1A, left panel). We have previously demonstrated that these two RNA structures act in a cooperative manner: while mutation of xrRNA1 abolishes accumulation of sfRNA1, mutation of xrRNA2 greatly reduces the accumulation of both sfRNAs (10). However, to eliminate the production of both ZIKV sfRNAs, a deletion of the two xrRNA structures is necessary (ZIKV sfRNAnull, Figure 1A, right panel). The WT and sfRNAnull ZIKVs efficiently infect and propagate in C6/36 mosquito cells (Supplementary Figure S1), yielding high viral titers (more than 1×10^8 infectious particle/ml). Thus, these cells were used to produce viral stocks throughout this work. Infection of human A549 cells with each of the two viruses at multiplicity of infection (moi) of 5 resulted in a complete antigen-positive monolayer at 24-h post-infection (hpi) (Figure 1B). However, while the WT virus caused profound cytopathic effects (CPE) and cell death at 48 and 72 hpi, the sfRNAnull virus was efficiently eliminated from the cells after 48 h, and cells remained with no sign of CPE (Figure 1B). The efficient clearance of the mutant virus after infecting most of the monolayer was unprecedented and suggested a defect in the virus to control the cell antiviral response.

Infection kinetics with the WT and the sfRNAnull virus in A549 cells indicated similar viral RNA levels up to 16 hpi, while differences were observed after 18 hpi (Figure 1C). The accumulation of viral proteins, measured by WB, showed the progression of the infection of both viruses between 12 and 48 hpi (Figure 1D). In this regard, while the WT viral proteins dropped at 72 hpi due to extensive CPE, the reduction of viral proteins in the mutant was likely due to clearance of the virus (Figure 1D), as shown in Figure 1B. We then analyzed the innate antiviral response during infection with the two viruses. For this, we evaluated type I IFN production at the mRNA and protein levels. Type I IFN mRNA was measured by qRT-PCR, while the secreted protein was quantified by ELISA. Since IFN-β was the only type I IFN observed in A549 cells after ZIKV infection under our experimental conditions, we measured this cytokine. A significant induction of IFN-β mRNA was observed after infection with both viruses (Figure 1E). The WT induced approximately a 10-fold higher level of IFN-β mRNA than the sfRNAnull virus after 16 hpi (Figure 1E). Quantification of the secreted IFN-β protein in infected cell supernatants also showed a significant increase for the two viruses over time post-infection (Figure 1F). However, IFN-β protein was significantly lower in ZIKV WT compared to the sfRNAnull virus infection (Figure 1F). The higher expression of IFN-β mRNA but lower IFN-β protein produced in the WT ZIKV infection was striking, supporting the hypothesis that accumulation of sfRNAs interferes with IFN production at the translation or secretion level. Because previous studies performed in our laboratory and others (10,11,30) assessed IFN production by measuring mRNA induction, the effect observed here on IFN protein secretion may have been previously overlooked.

WT and sfRNA deficient ZIKV infection differentially induce PKR activation and eIF2α phosphorylation

Viral infection is associated to activation of stress pathways that can lead to translation inhibition by phosphorylation of the α-subunit of eIF2. Thus, we examined whether the differential downregulation of IFN-β protein expression observed with ZIKV WT vs the virus sfRNAnull was associated with the phosphorylation state of eIF2α. A549 cells were infected with each virus (moi of 5), and the phosphorylated form of eIF2α was evaluated over time after infection using immunofluorescence analysis (IFA). In the case of the WT virus, phosphorylated eIF2α (phospho-eIF2α) was detected in scattered cells at 6 hpi, and this was extended to most of the monolayer at 24 hpi (Figure 2A). In contrast, no sign of phospho-eIF2α was observed in ZIKV sfRNAnull infected cells, not even at 24 hpi when the cell monolayer was completely infected (Figure 2A). These results suggest a differential phosphorylation of eIF2α during the course of infection of the two viruses.

To confirm this observation, host and viral proteins were analyzed by western blots (WBs) at different times after infection (12, 24 and 36 hpi). Consistent with the IFA data, phospho-eIF2α was detected in cytoplasmic extracts of WT infected cells, while no phospho-eIF2α was observed in the

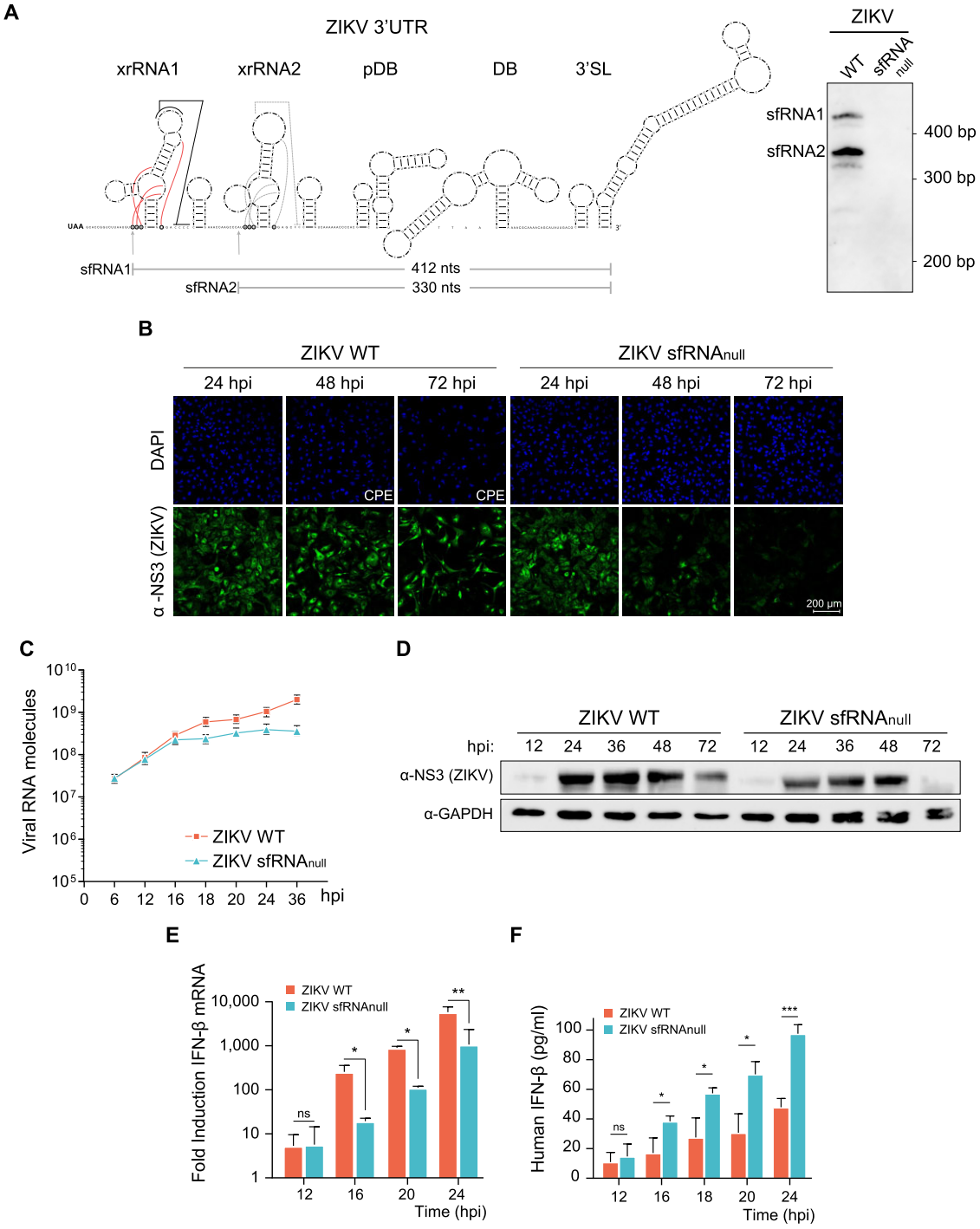

Figure 1. Role of ZIKV sfRNAs in inhibition of interferon production. (**A**) Schematic representation of ZIKV 3′UTR, highlighting the predicted RNA structures, including exoribonuclease-resistant RNAs 1 and 2 (xrRNA1 and xrRNA2), pseudo-dumbbell (pDB), dumbbell (DB) and 3′ stem-loop (3′ SL). The two main sfRNAs of 412 and 330 nucleotides are also shown. On the right, a northern blot illustrates the pattern of sfRNAs generated during ZIKV WT and sfRNAnull infections in A549 human cells at 24 h post-infection (moi = 5). (**B**) Propagation of ZIKV WT and sfRNAnull in A549 cells. Representative images from IFA using anti-NS3 antibodies and DAPI staining in A549 cells infected at moi of 5 with WT or sfRNAnull virus. Cytopathic effect (CPE) was observed with the WT virus at 48 hpi as indicated. (**C**) Accumulation of ZIKV RNA genome over time in the infected cell, assessed by RT-qPCR for both WT and sfRNAnull. The data represent the means with standard deviation (SD) of three biological replicates performed in parallel each in duplicates for RT-PCR measurements. Statistical significance was determined using an unpaired t-test, showing significant differences in replication after 16 h post-infection (hpi). (**D**) Viral protein accumulation over time in WT and sfRNAnull ZIKV infection in A549 cells at moi of 5. Cell extracts harvested at different hpi were used for the detection of the viral protein NS3, as well as glyceraldehyde-3-phosphate dehydrogenase (GAPDH), as indicated. (**E**) WT ZIKV infection induces IFN-β mRNA expression but limits IFN-β protein secretion. IFN-β mRNA levels measured by RT-qPCR relative to GAPDH mRNA and expressed as fold change respect to the non-infected control, in cells infected with WT or sfRNAnull ZIKVs at moi of 5. Measurements are shown at different time points after infection (hpi). (**F**) Levels of IFN-β protein measured in supernatants by ELISA from A549 cells infected with WT or sfRNAnull ZIKVs at moi of 5. Measurements are shown at different time points after infection (hpi). The data represent means with standard deviation (SD) of three independent experimental replicates. For both panels, statistical significance was determined using an unpaired t-test, with P values indicated as follows: $*P \leq 0.05$; $**P \leq 0.01$; $***P \leq 0.001$ and ns, not significant.

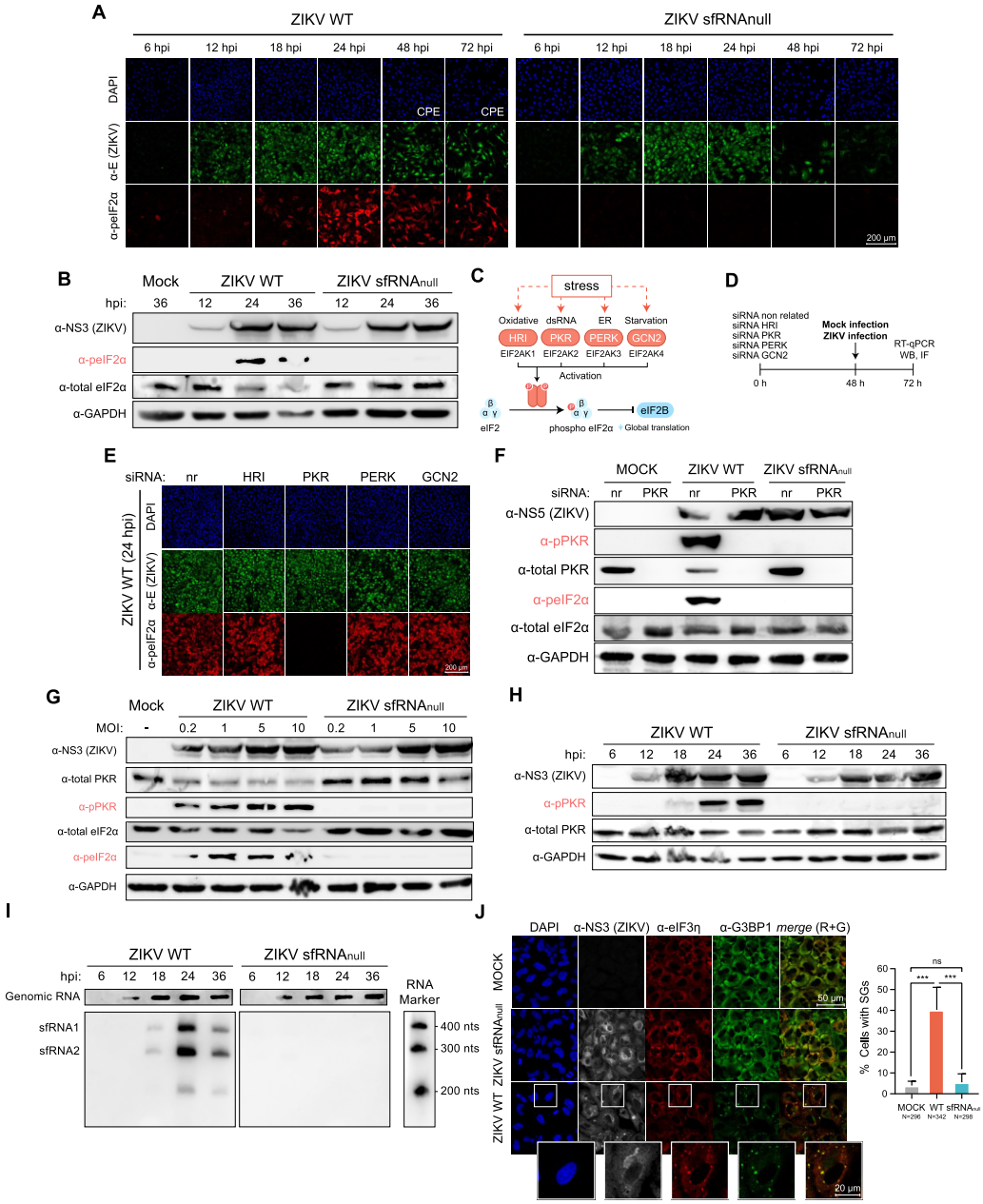

Figure 2. Differential eIF2α phosphorylation and PKR activation in WT and sfRNAnull ZIKV infections. (**A**) Phosphorylation of eIF2α in infected A549 cells. Representative images of IFA using α-Envelope (**E**) viral protein, α-phospho-eIF2α (peIF2α), and DAPI staining in A549 cells infected with WT or sfRNAnull ZIKVs (moi of 5). On the top, different times post-infection (hpi) are indicated, cytopathic effect (CPE) is also indicated. (**B**) Differential eIF2α Phosphorylation by WT and sfRNAnull ZIKV as a function of time post infection. WB analysis showing levels of phosphorylated eIF2α at 12, 24 and 36 hpi from cells infected with WT or sfRNAnull ZIKVs. The viral protein NS5 is also displayed, along with phospho-eIF2α (peIF2α), total eIF2α and glyceraldehyde-3-phosphate dehydrogenase (GAPDH). (**C**) Schematic representation of convergent eIF2α phosphorylation by different kinases (EIF2AKs) that results in global translational arrest. Stress conditions lead to autophosphorylation, dimerization and activation of the four kinases shown. (**D**) Experimental design for silencing each of the EIF2AKs in A549 cells that were subsequently used for ZIKV infection, as indicated. (**E**) PKR is required for eIF2α phosphorylation in ZIKV infections. Representative images from IFA using α-E protein, α-phospho-eIF2α (peIF2α), and DAPI staining in silenced A549 cells for each kinase, as indicated. Cell were infected with moi = 5 and images obtained at 24 hpi. (**F**) PKR silencing reduces eIF2α phosphorylation in WT ZIKV infection. WB analysis of A549 cells PKR KD or non-related control (nr), infected with WT or sfRNAnull ZIKVs at moi = 5. Cell extracts harvested at 24 hpi were used for detection of the viral protein NS5, phospho-PKR (pPKR), total PKR, peIF2α, total eIF2 α and GAPDH, as indicated. (**G**) ZIKV WT infection triggers PKR activation at 18 hours post-infection. WB analysis of A549 cells infected over time with WT or sfRNAnull ZIKVs at moi of 5. Cell extracts were harvested at the indicated hpi, showing pPKR, total PKR, viral protein NS3 and GAPDH. (**H**) Accumulation of sfRNAs over time after infection with the WT and the sfRNAnull ZIKV. Northern Blot analysis showing on the top the genomic viral RNA and on the bottom sfRNAs as a function of time post infection, using the same samples shown in section G of this Figure. (**I**) ZIKV sfRNAnull does not activate PKR even when infection is at high moi. WB analysis of A549 cells infected with WT or sfRNAnull ZIKVs at mois of 0.2, 1, 5 and 10, as indicated on the top. Cell extracts obtained 24 hpi were used to detect pPKR, total PKR, peIF2α, total eIF2α, viral NS3 and GAPDH. (**J**) WT ZIKV infection triggers stress granules assembly. Left: Representative images from IFA of infected A549 cells. DAPI staining, anti-NS3 antibodies, anti-eIF 3η and anti-G3BP1 are shown. The merge of red and green channels is also indicated. Right: A bar plot shows the percentage of cells with SGs in A549 cells infected with WT or sfRNAnull ZIKVs at moi = 5 at 24 hpi. The number of cells scored in each condition is indicated at the bottom. SGs were defined by granules with G3BP1 and eIF3η signal. Statistical significance was determined using an unpaired *t*-test, with *P* values indicated as follows: ***$P \leq 0.001$; and ns, not significant.

sfRNAnull infection (Figure 2B). In addition, extracts from cells infected with this mutant showed similar levels of total eIF2α (Figure 2B). Phosphorylation of eIF2α is mediated by the activation of at least one of the following four kinases: PERK (responsive to accumulation of misfolded proteins in the endoplasmic reticulum), PKR (responsive to viral RNA), HRI (responsive to heme deficiency and oxidative mitochondrial stresses), and/or GCN2 (responsive to amino acid deprivation) (Figure 2C). Different reports indicate that PKR and/or PERK are activated during infection with different flaviviruses (31–35). To evaluate the kinase/s responsible for eIF2α phosphorylation during WT ZIKV infection, we knocked down (KD) each of the four kinases (Figure 2D). The reduction of mRNA for each kinase was confirmed by qRT-PCR (Supplementary Figure S2A). KD cells were then infected with WT ZIKV, and the phospho-eIF2α was examined by IFA (Figure 2E). We observed that PKR silencing abolished eIF2α phosphorylation in infected cells, while silencing PERK, GCN2, or HRI showed similar phospho-eIF2α levels to those in cells treated with the non-related siRNA control (Figure 2E). Because PERK activation was previously associated to flavivirus infection, as control, we evaluated the levels of PERK in PKR-KD cells. The WBs showed the presence of this kinase in PKR-KD and control cells (Supplementary Figure S2B).

To further evaluate whether the differential phosphorylation of eIF2α in cells infected with viruses producing or not sfRNAs was due to selective PKR activation, we infected A549 cells, either PKR KD or control, with the two viruses and assessed PKR and eIF2α phosphorylation by WBs (Figure 2F). In cells treated with the non-related (nr) siRNA control, the presence of phospho-eIF2α and phospho-PKR was evident in infections with the WT virus at 24 hpi (Figure 2F). In PKR KD cells infected with WT ZIKV, eIF2α was not phosphorylated, supporting the role of PKR in this process. As expected, infections with sfRNAnull virus did not show phosphorylation of PKR or eIF2α, either in the PKR KD or control cells. PKR activation by ZIKV was also evaluated in different human cells lines (Huh-7 and HEK 293T). In agreement with the observation in A549 cells, infection with ZIKV WT but not with the mutant sfRNAnull showed PKR activation (Supplementary Figure S2C).

To evaluate a possible impact of the difference in replication between the WT and sfRNAnull viruses on the level of PKR activation, we used increasing multiplicities of infection (0.2, 1, 5 and 10) in A549 cells. Cell extracts from each condition at 24 hpi were used to evaluate the total level of PKR, as well as the phosphorylated forms of eIF2α and PKR. While phospho-eIF2α and phospho-PKR were observed upon infection with every moi used for the WT ZIKV, no phosphorylation of these proteins was detected with sfRNAnull virus infection, not even at moi of 10 (Figure 2G). Similar results were observed with increasing mois when infecting Huh-7 cells (Supplementary Figure S2D). These results further confirm that eIF2α is phosphorylated by PKR upon ZIKV WT infection but not with the virus that does not produce sfRNAs.

To further evaluate the temporal correlation between PKR phosphorylation and sfRNA accumulation during ZIKV infection, we performed kinetic studies assessing sfRNA generation by northern blots (NB) and kinase activation by WB, in parallel. PKR phosphorylation was evident at 18 hpi (Figure 2H), which correlates with the detection of sfRNAs in the WT virus (Figure 2I). Furthermore, the mutant sfRNA virus did not produce any sfRNAs throughout the duration of the infection (Figure 2I).

Stress granules (SGs) are structures composed of cellular mRNAs and stalled translation preinitiation complexes formed in stress conditions associated to translation inhibition (36,37). Thus, we evaluated whether SGs are induced in cells infected with WT or sfRNA deficient virus. Cells infected with each virus were used for IFA analysis labeling with antibodies for G3BP1 (an SG marker) and eIF3n (a preinitiation complex of translation marker). We observed an increased number of condensates containing G3BP1 and eIF3n in WT ZIKV infections (Figure 2J), suggesting induction of SGs. The granules detected in infected cells also contained the TIAR protein, often found in SGs (Supplementary Figure S2G). In contrast, no condensates with these host proteins were observed in infections with the sfRNA deficient virus. To assess whether the translation inhibition caused by PKR activation was associated with SGs formation during WT ZIKV infection, we quantified the number of cells with SGs in infected PKR KD cells. This analysis indicated that PKR KD also abolishes SGs formation (Supplementary Figure S2H), suggesting the involvement of both PKR and sfRNAs in SG formation during ZIKV infection.

In summary, ZIKV infection induces PKR activation, which leads to eIF2α phosphorylation and translational arrest in a process that is associated to the accumulation of viral sfRNAs.

sfRNA-dependent PKR activation enhances viral replication

Although PKR is described as an antiviral sensor, our data suggest that ZIKV exploits PKR activation by sfRNAs to control the antiviral response. To investigate this counterintuitive possibility, we analyzed the impact of silencing PKR on WT or sfRNAnull ZIKV replication. First, we determined that PKR KD did not affect cell growth by measuring cellular ATP in control and PKR silenced cells in the conditions used for viral infections (Supplementary Figure S3A). Then, PKR KD A549 cells were infected, and viral replication was assessed by measuring viral genome accumulation. As a control, we downregulated RIG-I, an antiviral protein whose functions against flaviviruses is well documented (38) (Figure 3A). The reduction of PKR and RIG-I mRNA levels was confirmed using qRT-PCR for each gene (Supplementary Figure S3B). RIG-I KD led to a significant increase in ZIKV replication for both WT and sfRNAnull viruses (Figure 3B), supporting its antiviral role irrespective of sfRNA accumulation. In contrast, PKR KD significantly reduced WT ZIKV replication, while the sfRNA-deficient virus was insensitive to PKR KD (Figure 3B). These results support the idea that PKR displays a proviral activity during infection with a ZIKV that accumulates sfRNAs.

To extend this observation, we conducted viral replication kinetics assessing the accumulation of viral RNA and the production of infectious particles in cells with or without PKR. In PKR KD cells, we observed a significant reduction in the WT virus genomic RNA at 18 hpi, while the sfRNAnull virus was unaffected (Figure 3C). Supernatants were harvested at 24 hpi under each condition and used to quantify the amount of secreted infectious particles. Consistent with viral RNA measurements, the WT ZIKV showed a reduction in the number of focus-forming units produced from cells lacking PKR (Figure 3D). In contrast, the production of infectious particles by the sfRNA-deficient virus was unaffected in PKR KD cells. To

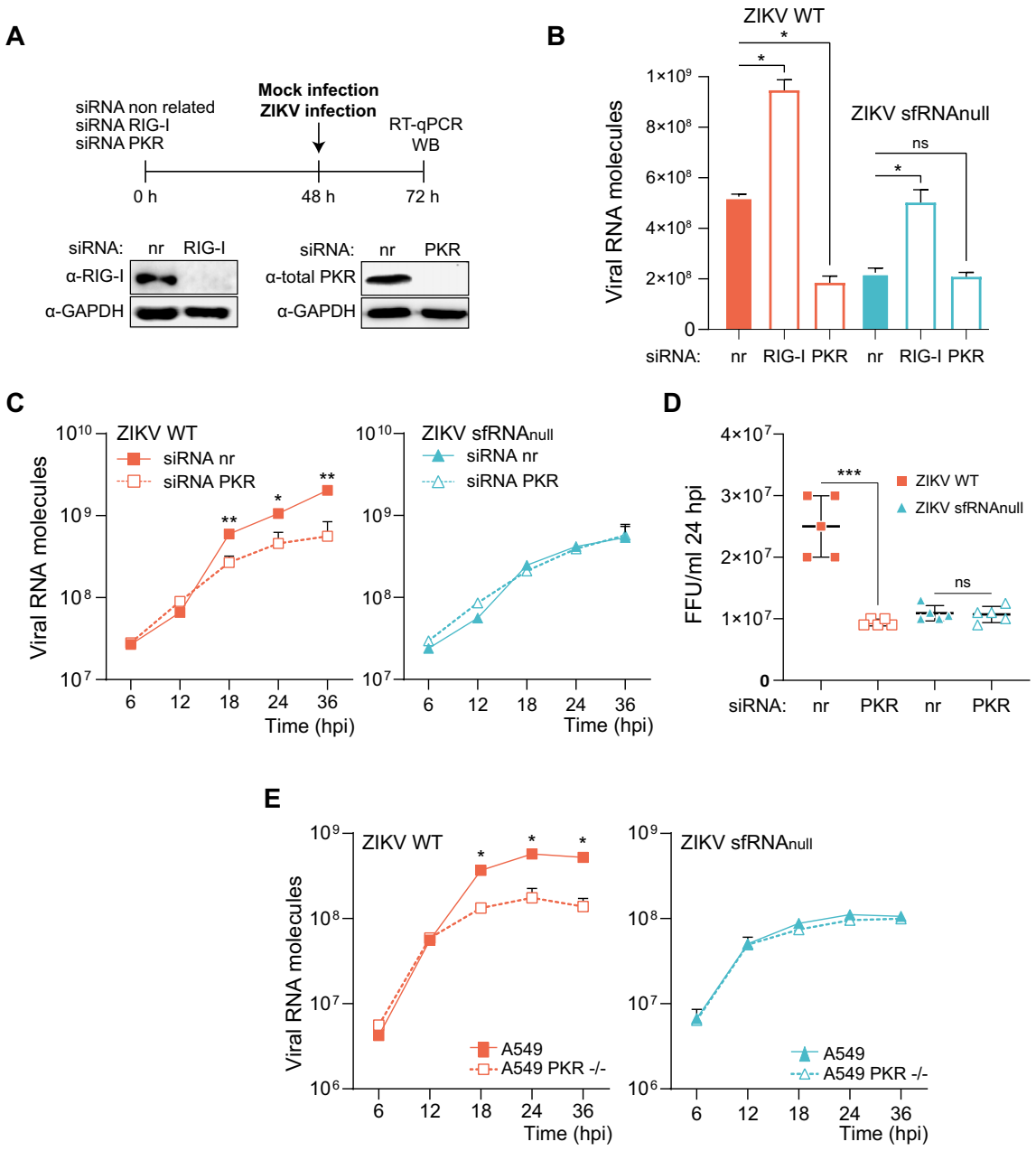

Figure 3. PKR activation by ZIKV sfRNAs displays a proviral function. (**A**) Silencing PKR and RIG-I. Top: Experimental design for silencing PKR and RIG-I. A non-related (nr) siRNA control was included. Cells were infected with mock, WT, or sfRNAnull ZIKV 48 hpt of the siRNAs and viral replication was evaluated 24 hpi. Bottom: western blot (WB) analysis of silenced A549 cells evaluating the levels of RIG-I and PKR. For this, cell extracts were harvested at 48 h post-transfection (hpt). (**B**) PKR KD reduces ZIKV replication. Quantification of viral RNA by RT-qPCR for infections with the WT or sfRNAnull viruses, in silenced A549 cells for RIG-I, PKR or non-related control (nr), as indicated for each case. The data represent means with standard deviation (SD) of three independent experimental replicates. Statistical significance was determined using an unpaired *t*-test, with *P* values indicated as follows: $*P \leq 0.05$ and ns, not significant. (**C**) Kinetics of ZIKV WT and sfRNAnull replication in PKR KD cells. ZIKV RNA genome accumulation is shown as a function of time assessed by RT-qPCR for the WT (left panel) and sfRNAnull (right panel) in PKR KD and control (nr) A549 cells, as indicated. The data represent means with standard deviation (SD) of three experimental replicates. Statistical significance was determined using an unpaired *t*-test, with *P* values indicated as follows: $***P \leq 0.001$; and ns, not significant. (**D**) Production of ZIKV infectious particles in PKR KD A549 cells. Viral titers measured by Focus Forming Units/ml (FFU/ml) are shown. The data represent means with standard deviation (SD) of five independent experiments performed the same day; each point was measured in triplicates. Statistical significance was determined using an unpaired *t*-test, with *P* values indicated as follows: $***P \leq 0.001$; and ns, not significant. (**E**) Kinetics of ZIKV WT and sfRNAnull replication in PKR-/- A549 cells. ZIKV RNA genome accumulation is shown as a function of time assessed by RT-qPCR for the WT (left panel) and sfRNAnull (right panel) in control and PKR-/- A549 cells, as indicated. The data represent means with standard deviation (SD) of four experimental replicates. Statistical significance was determined using an unpaired *t*-test, with *P* values indicated as follows: $***P \leq 0.001$; and ns, not significant.

confirm our findings, we used a different model by employing A549 cells PKR-/-. Replication of ZIKV WT and sfRNAnull in these cells resembled that observed with PKR KD. While the sfRNAnull virus replication was not affected, the WT virus was reduced >4-fold in the absence of PKR (Figure 3E).

Furthermore, we assessed the impact of translation inhibition on ZIKV replication by pharmacological intervention. We used a small molecule that acts as integrated stress responses (ISR) inhibitor (ISRIB), which rescues translation in the presence of phosphorylated eIF2α, by enhancing IF2B GEF activity (39–41). Addition of the drug, mimicked the phenotypes observed in cells PKR KD or KO, reducing the level of WT virus replication at 24 hpi, without altering the replication of the sfRNA deficient mutant (Supplementary Figure S3C).

Together, these results support the idea that PKR displays a proviral activity during ZIKV infection by a mechanism related to sfRNA-production.

ZIKV sfRNAs mediate PKR activation in the absence of other viral components

Because PKR activation was observed in ZIKV infection only when sfRNAs were produced, we examined whether sfRNAs could induce PKR activation. For this, *in vitro*-synthesized sfRNAs resembling those found in ZIKV-infected cells (sfRNA1 and sfRNA2) were transfected into A549 cells, and PKR auto-phosphorylation was evaluated. Since viral genome degradation by XRN1 results in 5′-monophosphorylated RNA products (5′-p sfRNAs), we treated the 5′-tri-phosphate RNAs generated by *in vitro* transcription with a 5′ pyrophosphohydrolase to produce the 5′-p sfRNAs. Cells were transfected with 5′-p sfRNAs or poly I:C, a synthetic analog of double-stranded RNA, and PKR activation was analyzed in cytoplasmic extracts by WB (Figure 4A). We detected phospho-PKR in the positive control transfected with poly I:C at 1 and 4 h post-transfection. Transfection of the 5′-p sfRNAs also induced PKR phosphorylation at later time (Figure 4A, top panel), suggesting that these molecules can activate PKR in the absence of other viral components. An extended time course showed that PKR activation by 5′-p sfRNA was detected at 16 h post-transfection (Figure 4A, bottom panel).

To map the structural elements within the sfRNAs that may function as PKR activators, we designed a battery of RNA molecules with deletions of the conserved RNA structures of the viral 3′UTR. Molecules with deletions of xrRNA1, xrRNA1/2, pDB, DB or the 3′SL structures were obtained (Figure 4B), and used to assess PKR auto-phosphorylation. A549 cells were transfected with each 5′p-RNA, and phospho-PKR was evaluated by WB analysis (Figure 4C). RNAs containing one or both xrRNA structures (5′p-sfRNA1 or 5′p-sfRNA2) activated PKR, while RNAs with a deletion of both elements (ΔxrRNA1/2) eliminated this function. The lack of PKR activation with this mutant also indicated that no side products of the transcription induced phosphorylation of the kinase. In addition, RNAs lacking the pDB, DB or the 3′SL retained the ability to activate PKR (Figure 4C). This observation suggests that at least one xrRNA in the 5′p-sfRNA molecule is required for inducing PKR phosphorylation.

Because the presence of xrRNA structures confers stability to the RNA molecule by providing resistance to XRN1 exoribonuclease degradation, it is possible that the 5′p-ΔxrRNA1/2 molecule failed to activate PKR due to its reduced RNA stability in the cell. To test this possibility, we introduced a mutation that eliminated the pseudoknot (PK) interaction in both xrRNAs (5′p-sfRNA PKmut), debilitating the two RNA structures that halt XRN1, rendering molecules that are susceptible to degradation, while retaining the stem loops (SL1 and SL2) (Figure 4D). Thus, the question was whether this PKmut RNA molecule that was proposed to be susceptible to XRN1 degradation was able to activate PKR.

First, to confirm that 5′-sfRNA-PKmut was indeed susceptible to XRN1 degradation, we conducted an *in vitro* enzymatic assay with recombinant XRN1 enzyme. Two controls were included: the sfRNA1 molecule (XRN1 resistant) and the one carrying a deletion of both xrRNAs (ΔxrRNA1/2, XRN1 susceptible). These RNA molecules were incubated in the presence or absence of XRN1, and the resulting products were analyzed by agarose gel electrophoresis (Figure 4E). While the 5′-p sfRNA1 resisted degradation, the other two molecules (the one with the deletion 5′p- ΔxrRNA1/2 or the one with the mutated PKs, 5′p-xrRNAs PKmut) were susceptible to XRN1 degradation. Then, the two susceptible RNA molecules, the 5′p-ΔxrRNA1/2 and 5′-p xrRNAs PKmut, were transfected into cells and phospho-PKR was assessed. The data revealed that the 5′p-xrRNAs PKmut still activated PKR, while the 5′p-ΔxrRNA1/2 did not (Figure 4F). These results collectively suggest that RNA elements present in the xrRNA structure are necessary for PKR activation, however, this function appears to be independent of these molecules' ability to halt XRN1 degradation.

Although the results indicate that viral sfRNAs can trigger PKR activation in the absence of other viral components, further research will be needed to define the potential involvement of other cellular components in the process.

Viral RNA structures in sfRNAs but not in the viral genome correlate with PKR activation

We have presented evidence indicating that RNA structures in the sfRNAs can activate PKR. However, it remains possible that the xrRNAs structures present in the 3′UTR of the viral genome could also activate this kinase, independently of sfRNA formation. To evaluate this possibility, we examined the level of PKR phosphorylation upon infection with different ZIKV mutants that either contain or lack xrRNAs in the viral genome and produce varying levels of sfRNAs. We employed three viral mutants, containing a deletion of xrRNA1 (ΔxrRNA1), xrRNA2 (ΔxrRNA2) or both xrRNA1 and xrRNA2 (sfRNAnull). Infection with ZIKV-ΔxrRNA1 results in the accumulation of large amounts of sfRNA2, whereas infection with ZIKV-ΔxrRNA2 results in minimal accumulation of sfRNAs, due to the cooperativity between different elements in the 3′UTR previously reported (10). As control for this experiment, we also included the sfRNAnull virus (ΔxrRNA1-xrRNA2), which does not produce sfRNAs. We infected A549 cells with either the WT ZIKV or each of the three mutant viruses, and assessed whether they induced PKR phosphorylation. For this experiment, viral stocks were generated in C6/36 cells and used to infect A549 cells at moi of 2 (Figure 4G). The comparison between ZIKV-ΔxrRNA1 and ZIKV-ΔxrRNA2 is particularly relevant, as both mutants contain one intact xrRNA structure in the viral genome, xrRNA1 or xrRNA2, potentially capable of inducing PKR activation, but only the ΔxrRNA1 virus produces substantial amounts of sfRNA (Figure 4G, bottom panel). We evaluated the infection levels by IFA and analyzed the cell extracts of mock or infected cells by

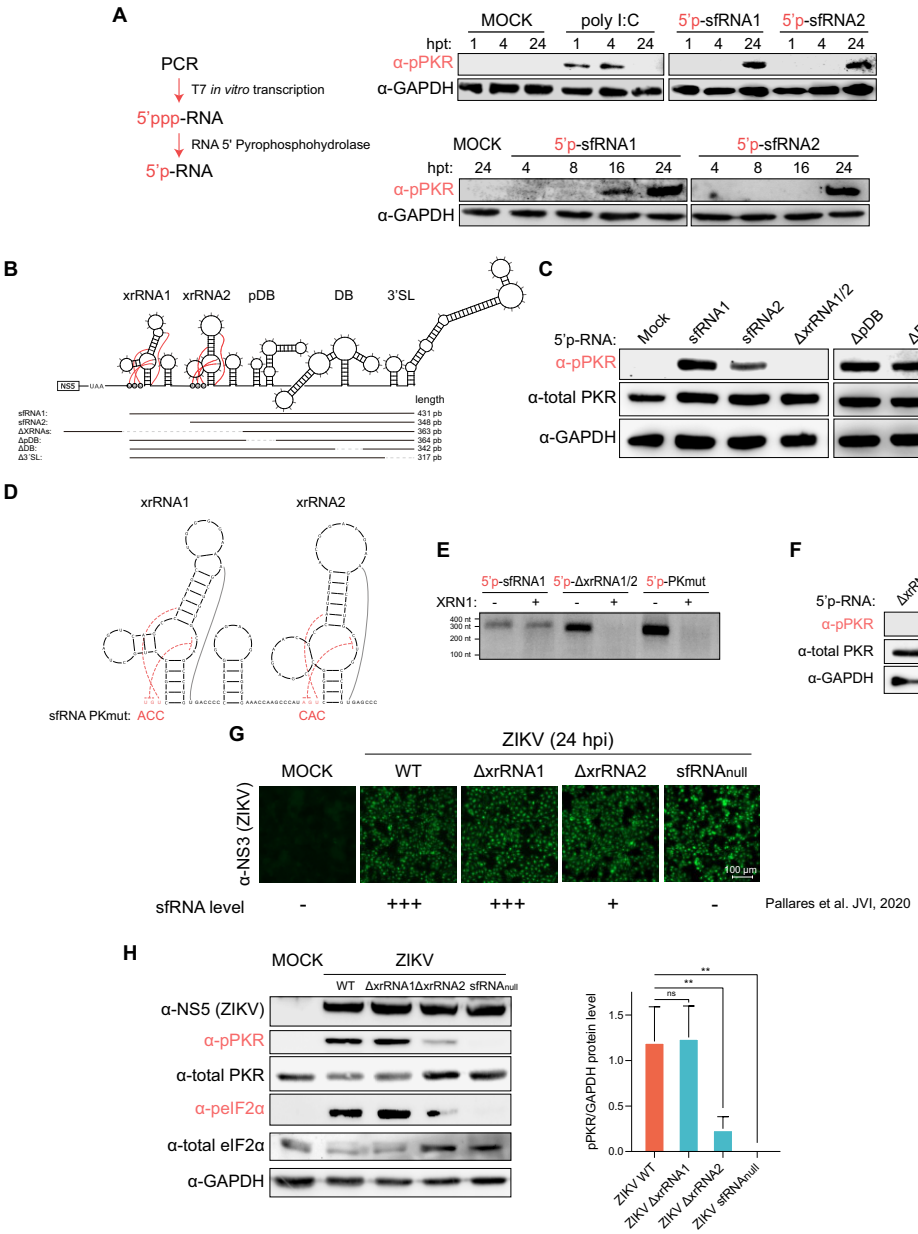

Figure 4. ZIKV sfRNAs mediate PKR activation. (**A**) Transfection of *in vitro* synthesized sfRNAs activates PKR. Left: Diagram illustrating the synthesis of *in vitro* sfRNAs with a monophosphorylated 5′ end (5′-p). Right: Western Blot analysis of A549 cells transfected with 400 ng/ml of poly I:C, 5′p-sfRNA1, or 5′p-sfRNA2. Cell extracts were harvested at different times post-transfection (hpt), showing phospho-PKR (pPKR) and GAPDH. The top and bottom panels show different time points. (**B**) Design of RNA structure deletions in sfRNAs. Schematic representation of ZIKV's 3′UTR, highlighting the predicted RNA structures, including exoribonuclease-resistant RNAs 1 and 2 (xrRNA1 and xrRNA2), pseudo-dumbbell (pDB), dumbbell (DB), and 3′ stem-loop (3′ SL). Designed RNAs with deletions are shown along with their predicted lengths. The mutant ΔXRNAs was designed to maintain a comparable length to the other mutants by including a sequence of the 3′ end of the ORF, as represented in the diagram. (**C**) Viral RNA structures that induce PKR activation. WB analysis of A549 cells transfected with 400 ng/ml of the *in vitro* transcribed 5′p-RNAs, including sfRNA1, sfRNA2, ΔxRNA1/2 (with a deletion in xRNA1-xRNA2), ΔpDB, ΔDB, and Δ3′SL, as indicated on the top. Cell extracts were harvested at 24 hpt and used for detecting pPKR, total PKR, and GAPDH, as indicated on the left. (**D**) Design of xrRNA mutation avoiding inhibition of exoribonuclease activity. Predicted structure of xrRNA1 and xrRNA2 showing the pseudoknots required for halting exoribonuclease activity and the mutations incorporated in the sfRNA PKmut RNA that disrupt the pseudoknots. (**E**) Enzymatic activity of recombinant XRN1 using different *in vitro* synthesized viral RNAs. Electrophoretic assay in agarose gel of products of XRN1 activity using 5′p-sfRNA1, 5′p-ΔxRNA1/2, and 5′p-PKmut, assessing the resistance of each RNA to the exoribonuclease activity. (**F**) WB analysis of A549 cells transfected with 400 ng/ml of 5′p- sfRNA1 or 5′p-PKmut RNAs. Cell extracts were harvested at 24 hpt and analyzed for pPKR, total PKR and GAPDH. (**G**) Viral infection of recombinant ZIKVs. Representative images from IFA depict ZIKV NS3 antigen positivity staining in A549 cells infected at moi of 2 with WT or mutant ΔxrRNA1, ΔxrRNA2, or sfRNAnull (with a deletion of both xrRNA1 and 2) at 24 hpi. At the bottom of the blot, as reference, the corresponding levels of sfRNA for each mutant is represented according to our previous work. (**H**) PKR activation by recombinant ZIKVs. Left: WB analysis showing proteins from A549 cells infected with WT or recombinant viruses at moi of 2. Cell extracts were harvested at 24 hpi, showing pPKR, total PKR, peIF2α, total eIF2α, viral NS5 and GAPDH. At the bottom of the blot, as reference, the corresponding levels of sfRNA for each mutant is represented according to our previous work. Right: Measurement of phospho-PKR level relative to GAPDH using blots obtained from five different experiments from A549 cells infected with WT or recombinant viruses at moi of 2 at 24 hpi. The data represent means with standard deviation (SD) of five experimental replicates. Statistical significance was determined using an unpaired *t*-test, with *P* values indicated as follows: $**P \leq 0.01$; and ns, not significant.

WB analysis. The data show that ZIKV-ΔxrRNA1 strongly activates PKR, while infection with ZIKV-ΔxrRNA2 results in very low levels of phospho-PKR (Figure 4H). Thus, both mutants retained one intact xRNA structure in the viral genome but only the one that produces sfRNAs activates PKR.

To extend these studies, we used two additional ZIKV mutants (mPK1 and mPK2) with disruption of each of the pseudoknots required for halting XRN1 degradation, which we have previously described (10). Infections with ZIKV mPK1 or ZIKV mPK2 produced disparate levels of sfRNAs, while the mPK1 generated large amounts of sfRNA2, the mPK2 infection was associated to a minimal amount of sfRNA (10). Here, we used these viruses to evaluate the induction of PKR phosphorylation (Supplementary Figure S4). Infection with ZIKV mPK1 showed PKR activation, while infection with ZIKV mPK2 showed very low levels of phospho-PKR (Supplementary Figure S4). The activation of PKR correlated with the ability of these ZIKV mutants to generate sfRNAs, however, it did not correlate with the presence of xrRNA structures in the viral genome (both viruses retained one intact xrRNA). It is relevant to link this observation with that obtained with the RNA molecule resembling the sfRNA with the PKs mutated showed above. In that case, transfection of the mutated mPK sfRNA induced PKR phosphorylation (Figure 4F).

The results support the idea that RNA structures in the xrRNAs present in the sfRNAs activate PKR, while the xrRNA elements present in the viral genome appear to be silent for PKR activation.

ZIKV sfRNAs modulate the host antiviral response by translational arrest

Given the evidence that sfRNAs mediate PKR activation and eIF2α phosphorylation, which reduces translation initiation, we undertook a global approach to examine global cellular translation in ZIKV infections. For this, we used RNA sequencing (RNA-seq) and ribosome profiling (Ribo-seq). A549 cells were infected with each of the two viruses, WT and sfRNA deficient, at moi of 5 and harvested at 20 hpi (Figure 5A). Paired libraries for RNA-seq and Ribo-seq were generated and sequenced (Figure 5B). Several sets of evidence revealed the high quality of our ribosome profiling. First, metaplot analysis showed the characteristic three-nucleotide periodicity of ribosome-protected fragments (RPFs) and depletion of RPFs after the stop codon (Figure 5D and Supplementary Figure S5A). Secondly, more than sixty percent of the RPFs of 29–32 nucleotide-long were in-frame, while the RNA input reads were uniformly distributed across the main coding sequence (Figure 5C). Third, >35 million reads mapped to mRNAs after filtering for non-coding RNAs (ribosomal RNAs, tRNAs and snoRNAs). Finally, the Ribo-seq and RNA-seq biological replicates displayed strong significant correlation and expected segregation in principal component analysis (Pearson, Supplementary Figure S5B and Supplementary Figure S5C).

To evaluate the impact of ZIKV infection on gene expression at the mRNA transcription and translation stages, we analyzed differential mRNA expression and RPFs for approximately 6000 highly expressed genes in cells infected with either the WT or sfRNAnull virus. Modest but significant differences at the mRNA levels were observed between WT vs. sfRNAnull infected cells ($P < 0.003$) (Figure 5E, left panel). However, strong translation repression was observed with the WT ZIKV in comparison to sfRNA null virus infection, as well as with the Mock infection (WT ZIKV vs sfRNAnull virus, $P < 2.2\ 10^{-16}$) (Figure 5E, right panel). This result reveals that accumulation of sfRNAs in ZIKV infection has an impact on the host cellular translation profile.

To assess the level of translation repression associated with the ZIKV producing sfRNAs, we calculated the translation efficiency (TE) for each of the 6000 genes. TE was determined by the ratio of RPFs to mRNA counts within the coding sequence (CDS). Cells infected with the WT virus showed reduced TE in comparison to the ones infected with the sfRNAnull virus (Figure 6A). Then, we evaluated the translation of a set of IFN-stimulated genes (ISGs) that were previously reported to have antiviral roles (42–44), and were detected in our Ribo-seq (Figure 6B). While several of these ISGs were up-regulated at the RNA level in cells infected with WT ZIKV compared to the sfRNAnull virus, their TEs were widely downregulated (Figure 6B and C). To rule out that the differences in TE could be attributed to differences at the RNA level (although the changes were in opposite direction), we generated a control group of genes for each condition to match the mRNA level of the ISGs (Figure 6D, left panel), and then interrogate the TE between ISGs and the control group in each condition. The TE of the ISGs was significantly reduced in cells infected with the WT ZIKV compared to the control group ($P < 0.001$, Figure 6D). In contrast, no significant difference in TE was observed between the ISGs and the control group in the mock-infected cells or in the sfRNAnull infected ones (Figure 6D). These results suggest that ZIKV represses cellular translation, leading to a lower TE for ISGs, as compared with that in cells infected with a virus that lacks production of sfRNAs. We also analyzed whether other genes involved in antiviral immune pathways were affected at the mRNA or translation level in cells infected with each virus. This analysis also supports repression at the TE level (Supplementary Figure S6).

In contrast to the global TE downregulation observed by ZIKV infection, the TE of the activating transcription factor 4 (ATF4) was upregulated in the WT ZIKV condition compared to the sfRNAnull infection (Figure 6B). ATF4 is known to be translationally upregulated in response to stress conditions due to the presence of upstream open reading frames (uORFs) (45). Under normal conditions, ATF4 translation is repressed, but under stress, the lower levels of initiation factors permit bypassing the uORFs, leading to ATF4 translation (Figure 6E). According to this, expression of downstream effectors, CHOP, GADD34 and ATF3, was significantly upregulated in the WT ZIKV infection (RNA fold change of 4.6, 3.4, 7.0, respectively, Figure 6F). To validate this observation, CHOP and GADD34 mRNA levels were measured in cells infected with WT or sfRNAnull ZIKV by qRT-PCR. We detected a significant increase of transcripts of these genes in the WT infection compared to that with the sfRNAnull virus (Figure 6G), supporting a differential activation of this stress pathway by the two viruses.

Translation efficiency of the viral genome was also evaluated. RNA levels, determined by RNAseq, indicated that WT infection at 20 hpi accumulated 3.8-fold more viral RNA that the sfRNAnull mutant (Figure 6H), which correlates with the qRT-PCR measurements at the same time (Figure 1C). The translation rate of the viral genome, evaluated by the number of RPFs, was 1.5 times higher in the WT-infected cells respect to the mutant virus. Therefore, the WT virus RNA displayed

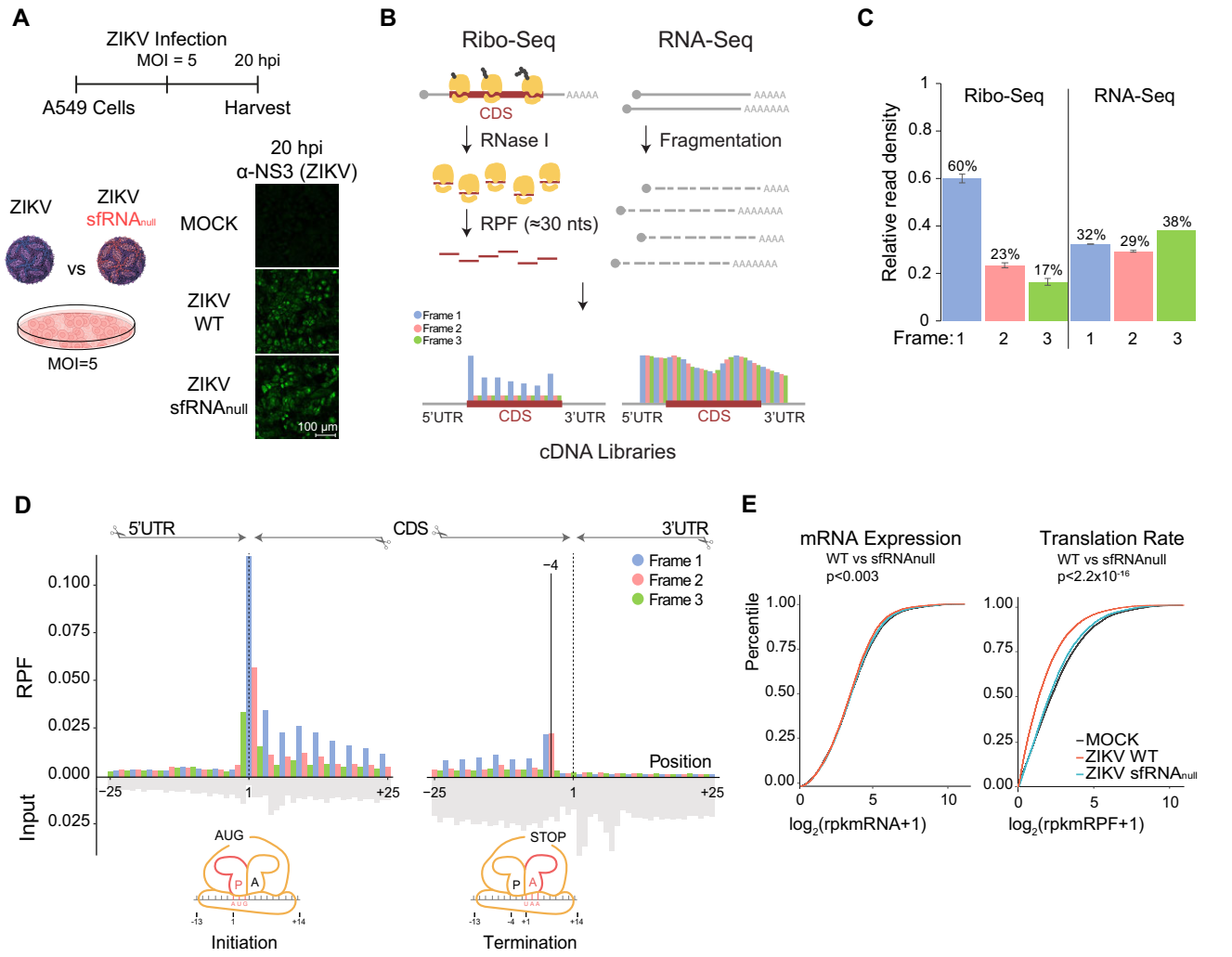

Figure 5. Impact of WT and sfRNAnull ZIKV Infection on Global Translation. (**A**) Top: Schematic representation of the protocol used to collect samples for ribosome profiling. Non-infected A549 cells and infected cells with an moi = 5 with WT or sfRNAnull ZIKV were harvested at 20 hpi for Ribo-seq and RNA-seq analysis. On the right, representative IFA images showing each condition used. (**B**) Experimental procedure for Ribo-seq (left) or RNA-seq (right). Left: Ribosome-bound mRNAs are isolated and treated with RNase I nuclease, preserving ribosome-protected fragments (RPFs) of approximately 30 nucleotides in length. These fragments result from the ribosome's resistance to digestion and exhibit precise positioning within the coding sequence of mRNAs. Right: RNA-seq captures mRNA fragments covering the entire transcript, including 5′ and 3′ untranslated regions (UTR). RNA-seq and Ribo-seq are performed in parallel to calculate translation efficiency. (**C**) RPFs and input reads mapped to a composite RefSeq transcript. RPFs primarily align with the coding sequence (CDS) and exhibit a 3-nucleotide periodicity. RPF reads are color-coded based on their position relative to the frame of the CDS, with most RPF reads in Frame 1. Input reads (in gray) map to both the UTRs and CDS, and do not have 3-nucleotide periodicity. The designation of the 1 position of the RPF is shown in both translation initiation and termination. (**D**) Distribution of ribosome footprints (RPFs) from Ribo-seq analysis and input reads from RNA-seq, as indicated on the top. Plots illustrate the proportion of RPFs or input reads aligned to the coding sequence of RefSeq genes at each position relative to the codon. RPFs predominantly map to the coding sequence (CDS) in frame 1 (blue). (**E**) ZIKV WT infection results in translational arrest. Cumulative plots of mRNA Expression and Translation Rate of genes in MOCK, ZIKV WT, or ZIKV sfRNAnull-infected cells. *P*-values are indicated and were obtained using the Wilcoxon rank-sum test.

lower TE (–2.5-fold) respect to the mutant virus, suggesting that the viral genome was also susceptible to translation arrest.

Translation downregulation of ISGs requires both sfRNAs and PKR

Our data support the notion of an unexpected ZIKV mechanism of controlling the immune response by viral derived sfRNAs that downregulate translation. To determine the impact of this translation inhibition on protein expression of antiviral genes, we examined ISG protein levels in cells infected with the WT or the sfRNAnull viruses by WBs. Cytoplasmic extracts of infected cells were used to assess the levels of the ISGs OAS3, TRIM5α and PKR, and in the same extracts the phosphorylated forms of PKR and eIF2α. Remarkably, although the replication of the WT virus was higher than the sfRNAnull virus, protein levels of OAS3 and TRIM5α were significantly lower in the WT ZIKV infection compared to that in cells infected with the virus deficient in sfRNAs production (Figure 7A). As control, to evaluate the RNA expression level of PKR, OAS3 and TRIM5a, qRT-PCRs were performed (Figure 7B). The results indicate that the mRNA levels are similar or even higher in the WT infection. This analysis supports the notion that the lower translation of these host proteins in the WT virus infection was not due to their RNA expression levels. These results validate the observation made with the ribosome profiling. Moreover, the level of total PKR and

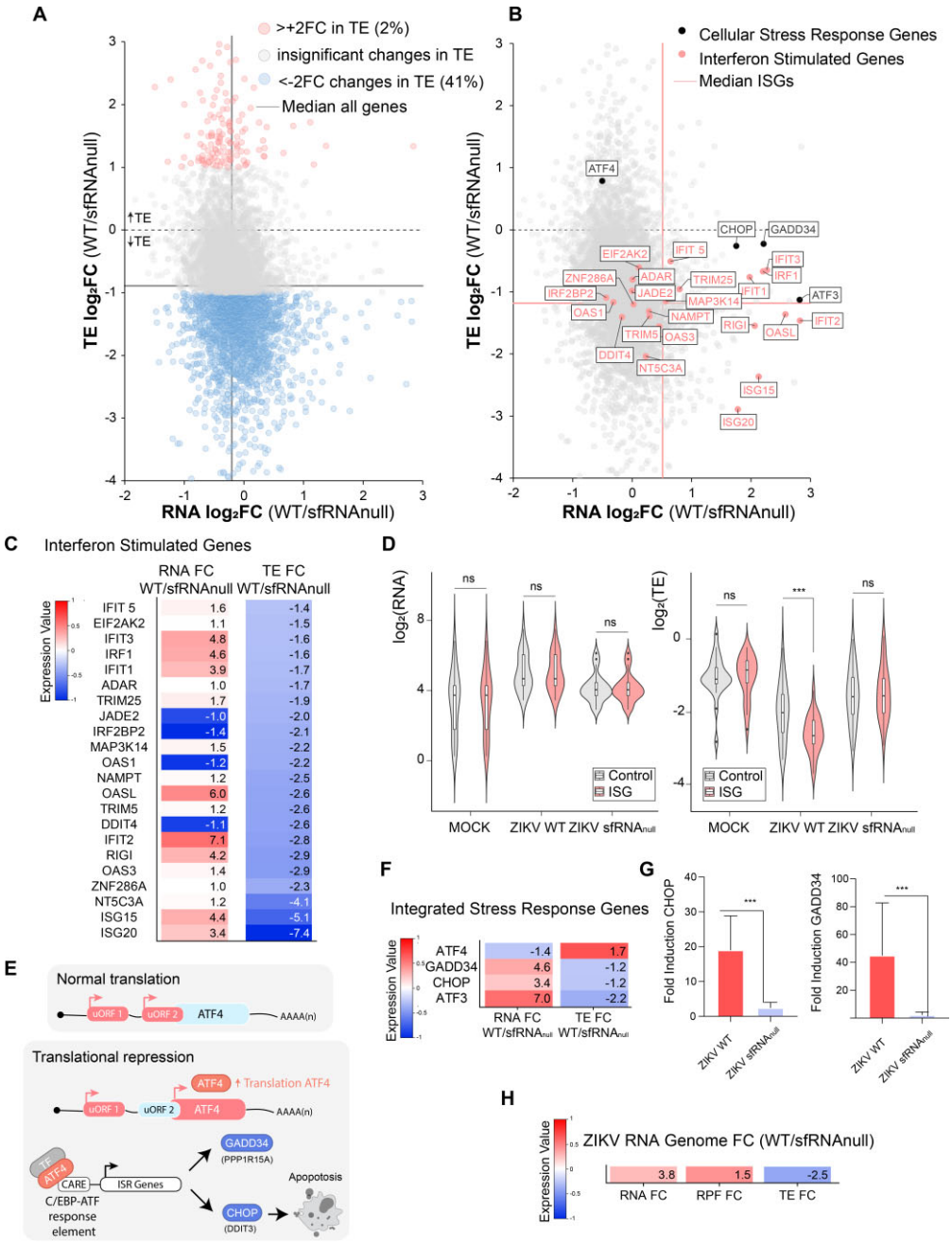

Figure 6. ZIKV Infection Induces Translational Arrest and Activation of the Integrated Stress Response. (**A**) ZIKV WT infection induces translational arrest. The plot displays differential RNA expression and translation efficiency (TE) of the top 6000 most expressed genes in WT and sfRNAnull ZIKV infections. Downregulated genes with less than −2 FC in TE are in blue, and genes with >2 FC in TE are in red. Median RNA and TE values for all genes are shown with grey lines. (**B**) Differential RNA and TE in WT and sfRNAnull ZIKV infections showing cellular stress response genes in black, and ISGs in red. Median values for ISGs are displayed with red lines. (**C**) Differential RNA expression and TE of ISGs in infected cells with ZIKV WT and sfRNAnull. Fold change values are shown. The color scale represents normalized RNA expression values across conditions (1: top gene, −1: bottom gene). Name of each ISG is indicated on the left. (**D**) ISG TEs are significantly downregulated during WT ZIKV infection. On the left, plots comparing a control group of genes with equal expression levels as the ISGs for Mock, WT and sfRNAnull ZIKV infections, calculated using a clustering k-nearest neighbor's algorithm. On the right, plots illustrating the TE of Control and ISGs for Mock, WT and sfRNAnull ZIKV infections, as indicated. Statistical significance was determined using a Wilcoxon rank-sum test, with P values indicated as follows: $***P \leq 0.001$; and ns, not significant. (**E**) Schematic representation of transcription factor ATF4 translation regulation. Translation of upstream ORFs (uORFs) takes place under normal conditions, while translation of ATF4 takes place during stress conditions. In this case, decreased translation factor levels cause the ribosome to bypass uORFs, allowing ATF4 translation. (**F**) ZIKV WT infection activates the integrated stress response (ISR) pathway. Differential RNA expression and TE of ISR genes for WT and sfRNAnull ZIKV infections. Fold change values are listed. The color scale represents normalized RNA expression values across conditions (1: top gene, −1: bottom gene). (**G**) Induction of CHOP and GADD34 mRNAs upon ZIKV infection. A549 cells infected with WT or sfRNAnull ZIKV at moi = 5 were used to assess expression at 24 h post-infection. Plot showing CHOP and GADD34 mRNA levels evaluated by RT-qPCR and expressed as fold induction relative to non-infected control, and relative to glyceraldehyde-3-phosphate dehydrogenase (GAPDH) mRNA. The data represent means with standard deviation (SD) of three independent experimental replicates. Statistical significance was determined using an unpaired t-test, with P values indicated as: $***P \leq 0.001$. (**H**) ZIKV genome TE. Fold change of viral RNA expression, Ribosome Protected Fragments (RPF) and viral translation efficiency (TE) for WT and sfRNAnull ZIKV infection; The color scale represents normalized expression values across conditions (1: top gene, −1: bottom gene).

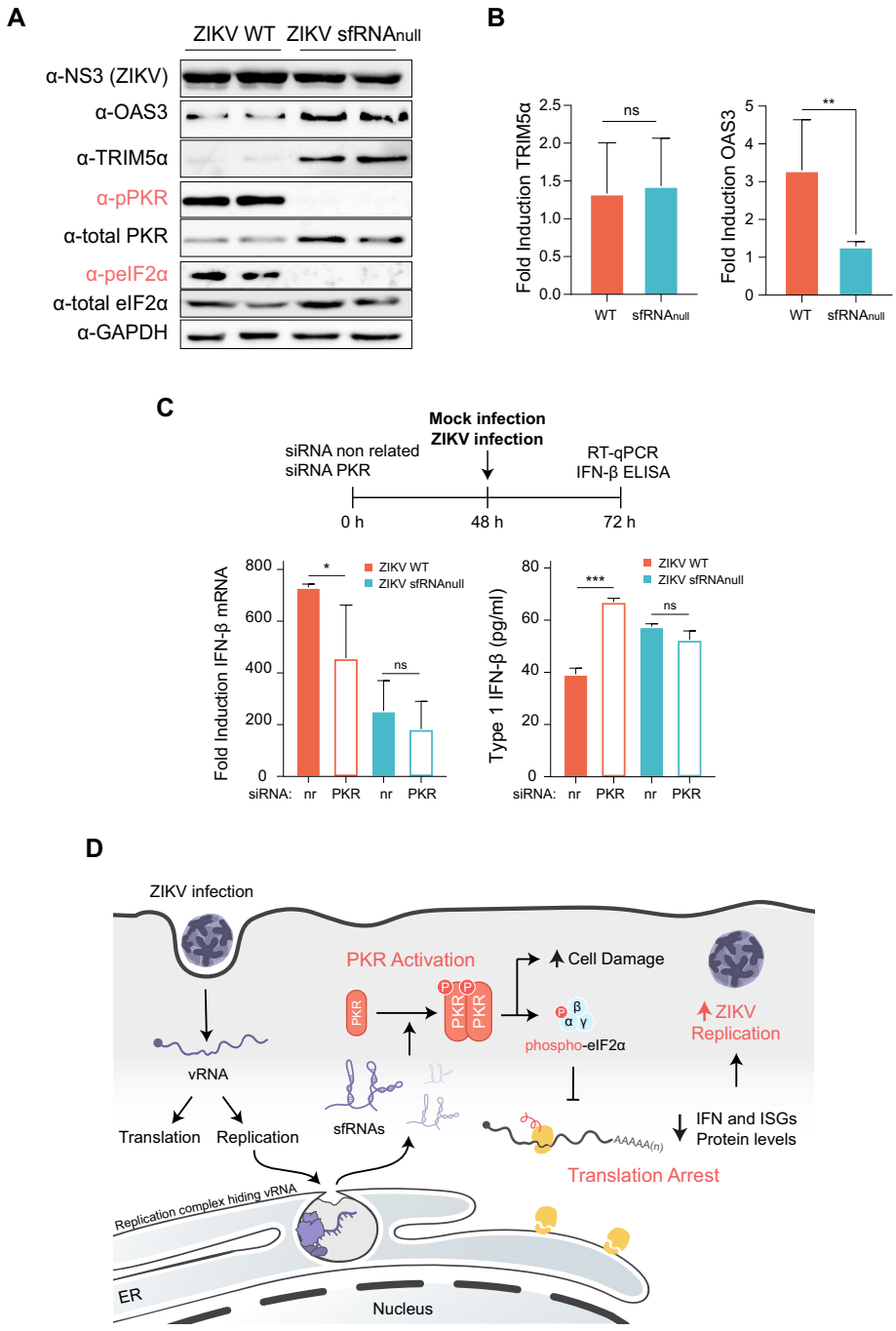

Figure 7. PKR activation by ZIKV sfRNAs inhibits interferon stimulated genes and IFN-β translation. (**A**) ZIKV sfRNAs are associated to translation repression of interferon stimulated genes (ISGs). WB analysis showing the level of ISGs from A549 cells infected with WT or sfRNAnull ZIKVs at moi of 5. Proteins detected are shown on the right: OAS3 and TRIM5α ISGs, phospho-PKR (pPKR), total PKR, phospho-eIF2α (peIF2α), viral NS3 and GAPDH. (**B**) Induction level of PKR, OAS3 and TRIM5α mRNAs in ZIKV infected cells. RNA levels were evaluated by RT-qPCR relative to glyceraldehyde-3-phosphate dehydrogenase (GAPDH) mRNA and expressed as fold induction relative to the non-infected control. The data represent means with standard deviation (SD) of three independent experimental replicates. Statistical significance was determined using an unpaired *t*-test, with *P* values indicated as follows: $*P \leq 0.05$; $**P \leq 0.01$; and ns, not significant. (**C**) IFN-β translation downregulation in ZIKV infection depends on PKR. Top: Experimental design for silencing PKR and infection with mock, WT, or sfRNAnull ZIKV at moi of 5. Bottom left, IFN-β mRNA levels measured by RT-qPCR relative to glyceraldehyde-3-phosphate dehydrogenase (GAPDH) mRNA and expressed as fold change respect to the non-infected control, in PKR KD or control (nr) A549 cells, infected with WT or sfRNAnull ZIKVs at moi of 5. Measurements are shown at 24 hpi. Bottom right panel, levels of IFN-β protein measured in the supernatants by ELISA from PKR KD or control A549 cells infected with WT or sfRNAnull ZIKVs at moi of 5. Measurements are shown 24 hpi. The data represent means with standard deviation (SD) of three biological replicates, each in duplicate. Statistical significance was determined using an unpaired *t*-test, with *P* values indicated as follows: $*P \leq 0.05$; $**P \leq 0.01$; $***P \leq 0.001$; and ns, not significant. (**D**) Model proposed for the mechanism of how ZIKV sfRNAs antagonize the innate antiviral response. During infection the viral genome (vRNA) is amplified inside replication complexes. The products of partial degradation of the vRNA leads to the accumulation of sfRNAs that exit these complexes and activate PKR. This kinase activation leads to phosphorylation of eIF2α and translational arrest. Activation of the PKR antiviral pathway instead of limiting viral infection, downregulates translation of antiviral genes, enhancing ZIKV replication and propagation.

total eIF2α were also markedly lower in the WT virus infection compared to that in cells infected with the mutant virus (Figure 7A). This decrease of total PKR and total eIF2 α proteins with the WT virus infection was also observed in different experiments presented above (for instance Figures 2F, 2G, S2F in A549 cells and Supplementary Figure S2B and S2D in other cell lines for PKR, and in Figures 2B, 4H and Supplementary Figure S2F for total eIF2α). This was unexplained at the beginning of this work, but correlates with the translation repression. Furthermore, ISG expression levels were analyzed in infections with ZIKV mutants that produce different levels of sfRNA. We compared infections with the WT, ΔxrRNA1, ΔxrRNA2 and ΔxrRNA1/2 (sfRNAnull). The data show an inverse correlation of ISG expression with PKR activation (Supplementary Figure S7). Together, these results indicate that the translational arrest during WT ZIKV infection displays a significant impact on ISG protein expression (Figure 7A).

We observed that WT ZIKV infection reduced protein secretion of type I IFN (Figure 1D). Also, we found that the lack of PKR was associated with decreased ZIKV replication and propagation (Figure 3C and D). Thus, we asked whether there is a link between these two observations. For this, we evaluated IFN-β production upon ZIKV infection in cells with or without PKR, using the same experimental setting employed in Figure 3A. Cells were transfected with siRNA for PKR KD, or a non-related siRNA control, and infected 48 h post-transfection (Figure 7C, top panel). We observed a reduced induction of IFN-β mRNA by WT ZIKV infection in PKR KD cells, likely due to the reduced viral RNA levels in this condition, which would be associated to a lower RIGI activation (Figure 7C, left panel). However, the levels of secreted IFN-β protein, measured by ELISA in the supernatants, significantly increased when compared with cells expressing PKR (Figure 7C, right panel). These results support the notion that downregulation of type I IFN protein production during ZIKV infection requires PKR. In contrast, in the infection with the sfRNA-deficient virus, no significant changes in the induction or secretion of type I IFN were observed upon PKR KD (Figure 7C and C).

Together, the data support a model in which sfRNAs play a role limiting the innate immune response by PKR activation and eIF2α phosphorylation, which leads to translation downregulation of antiviral genes that enhance viral replication (Figure 7D).

Discussion

Over the past decade, many laboratories have focused on investigating how flavivirus sfRNAs modulate antiviral responses and induce viral pathogenesis. However, much is still unknown regarding how sfRNAs interact and interfere with the host cell machinery for these functions. Using recombinant viruses and ribosome profiling of ZIKV infected human cells, we found that sfRNAs participate in repurposing the antiviral function of PKR to downregulate translation and modulate expression of antiviral genes. Our data provide a model of how the virus disarms cell defenses and exploit them to enhance viral infection.

RNA viruses have evolved a wide variety of mechanisms to counteract PKR activation. For instance, genome replication of various RNA viruses is associated to extensively rearranged intracellular membranes that hide dsRNA intermediates from PKR detection (46). Many RNA viruses encode proteins that bind and shield dsRNA from PKR sensing (47), while others suppress PKR by encoding proteins that inhibit the kinase function or promote PKR degradation (48,49). In the case of ZIKV and other flaviviruses, dsRNA intermediates of genome replication are sequestered in so called vesicle packets (VPs), which are membranous structures derived from the ER (50). While sfRNAs are generated inside VPs, they likely exit these structures to function in the cytoplasm of infected cells.

Our model supports the idea that ZIKV hides the viral genome during RNA synthesis, but produces and accumulates stable sfRNA molecules, which would exit the VPs and lead to PKR activation, eIF2α phosphorylation and translation arrest. The viral RNA structures that activate PKR are present in both, the 3′UTR of the viral genome and sfRNAs (Figure 4). However, we show that only the structures in sfRNA molecules activate PKR (Figure 4H and Supplementary Figure S4), providing evidence for the inaccessibility of the viral genome for PKR detection during ZIKV infection. We have previously shown that sfRNAs can be detected by Northern Blot about 12–18 h after ZIKV infection (10), which correlates with the timing of eIF2α and PKR phosphorylation observed in this work (Figure 2H and I). Paradoxically, instead of controlling virus infection, PKR activation enhances ZIKV replication, increasing infectious particle production and causing CPE.

Infections with ZIKV lacking the ability to produce sfRNAs or infecting PKR KD cells, show higher IFN-β protein secretion and ISG protein synthesis than the controls, suggesting that the interaction of the two components, sfRNAs and PKR, limits the antiviral response (Figures 1E, 7A and C). A function of ZIKV sfRNAs on type I IFN signaling has been recently reported using transcriptome analysis (11). Also, our previous work using DENV and ZIKV infected cells provided evidence of a potential role of sfRNAs in reducing type I IFN signaling (10,12). These previous observations evaluated type I IFN production by measuring mRNA expression, thus the possible impact of sfRNA generation on translation was not assessed. Here, we found that ZIKV infection limits IFN-β translation (Figure 1E). The Ribo-seq data show an impact of ZIKV infection on the TE of ISGs, regardless of the induction level of their mRNAs. In this regard, several ISGs displayed higher mRNA induction in WT ZIKV versus the sfRNA deficient virus, but yet their TEs were significantly reduced in the WT infection (Figure 6C). These data would indicate a direct impact of PKR activation on ISG translation. In addition, the higher induction level of ISGs upon WT ZIKV infection observed could be the consequence of activation of other pathways, besides type I IFN (44). We propose that the kinetics of the antiviral response, in terms of mRNA and protein expression, with respect to the timing of sfRNA accumulation and PKR activation, define the outcome of this multilayered process. Our results suggest that, in the case of ZIKV, these virus-host interactions favor viral replication. In agreement with our findings, a recent report has correlated PKR activation with DENV4 and ZIKV infections, also observing reduced viral replication in PKR knockout cells (32).

While it is common that RNA viruses rely on strategies to antagonize host innate immune defenses, it is less common to observe mechanisms that repurpose an antiviral factor to enhance viral replication, such as the one found here for PKR. In this regard, recent reports have revealed unexpected functions for antiviral factors during ZIKV infection. For instance,

RNase L, which typically detects and degrades viral RNA, was found to support the assembly of ZIKV replication complexes, enhancing virus production (51). This suggests that the virus has evolved a mechanism to subvert RNase L that supports viral replication. Another recent report has found the inhibition of mitophagy during ZIKV infection (52). In this regard, although mitophagy functions by eliminating damaged mitochondria to prevent the release of danger-associated molecular patterns, it has been shown that ZIKV degrades the host protein Ajuba, inhibiting mithophagy and amplifying the production of pro-inflammatory chemokines through PKR activation (52). Previous studies using hepatitis C virus (HCV), an immune evasion mechanism has been reported that also involves PKR activation. In this case, downregulation of ISG translation by PKR phosphorylation was observed upon external addition of type I IFN to HCV-infected cells (53). Since HCV employs a cap-independent translation mechanism with low sensitivity to eIF2α phosphorylation, viral translation remained efficient, highlighting an additional advantage of activating PKR. In the case of ZIKV, it is intriguing whether the translation arrest induced by PKR activation also affects viral translation. It is possible that the timing of sfRNA generation and PKR activation allows sufficient accumulation of viral proteins to support replication even in conditions of a reduced viral TE. Supporting this idea, the Ribo-seq data show that ZIKV genome TE was 2.5-fold lower upon PKR activation (Figure 6H). It is also possible that viral translation benefits from cellular translation arrest. It has been recently suggested that translation under the ZIKV 5′UTR, in the context of a reporter system, improves when cellular translation was inhibited (54). Although it is still unclear how ZIKV is able to translate its genome in low levels of translation initiation factors, we cannot rule out the possibility of a non-canonical initiation process. In this regard, previous studies have shown the presence of uORFs in the ZIKV genome (55), and improved translation of DENV and ZIKV was also observed when cap-dependent initiation was impaired (54,56).

Suppression of global translation has been previously suggested as a common feature of flavivirus infections, including ZIKV (57,58). However, it is unclear whether these viruses share similar mechanisms for translation arrest. In this regard, the xrRNA structures found to induce PKR phosphorylation are conserved and duplicated in mosquito-borne flavivirus genomes (54). We have previously reported that duplication of these RNA elements is relevant for DENV host-switching between mosquitos and human cells (59,60). We also found that disruption of these RNA structures, by adaptation to mosquito cells or by mutagenesis, is associated to low DENV fitness in human cells due to defects in controlling the host antiviral response (12). Based on the conservation of the RNA elements that are require for PKR phosphorylation, it will be important to investigate if PKR activation and the pathway to suppress ISG translation by sfRNAs is a common feature of mosquito-borne flaviviruses.

We observed that ZIKV infection induces the formation of SGs only when the virus produces sfRNAs, likely as a consequence of PKR activation and translation arrest (Figure 2J, Supplementary Figure S2G and S2H). In this regard, it has been previously reported that ZIKV infection inhibits SG formation when cells are exposed to external stressors like Arsenite or poly:IC (57). These observations suggest that different pathways can be activated under distinct stress conditions, such as viral infections or other stressors. The previously reported inhibition of SG formation could be due to downregulation of translation of SG proteins by ZIKV infection when a strong stressor is added post-infection. Using DENV, it has been shown that the SG proteins, including G3BP1/2 and CAPRIN1, play antiviral functions, and their depletion reduced type I IFN and other ISG translation (18,24). Interestingly, these SG proteins were found to bind DENV sfRNAs by interaction with xrRNAs structures. In this regard, it has been proposed that sfRNAs could serve as decoys for sequestering G3BP1 to limit the antiviral response. It will be important to evaluate a possible link between the DENV association with SG proteins and the PKR-dependent SG formation during ZIKV infection. For Mengovirus, another RNA virus, it has been reported that G3BP1, CAPRIN1 and PKR form a complex that activates PKR, which triggers an antiviral response (61). It is fascinating how different RNA viruses interact with the same set of host proteins with opposing outcomes, evasion or activation of host defenses. SGs have been associated with multiple functions during infection. They have been implicated in preventing excessive activation of dsRNA-induced innate immune signaling and also limiting viral replication. In this regard, it has been proposed a role for SG as safeguards for cell homeostasis, functioning as buffers to raise the threshold for apoptosis (62).

ZIKV infection leads to activation of the ISR (Figure 6F and G), which is associated to mechanisms to resolve the stress and avoid apoptosis, such as the role of GADD34 in dephosphorylation of eIF2α. However, the massive activation of eIF2α observed during ZIKV infection appears to be dysregulated, which could be the cause for cell damage and CPE. It has been recently reported that ZIKV sfRNA accumulation promotes apoptosis of neural progenitor cells in human brain organoids, leading to their disintegration (11). In infected human placental cells, sfRNA inhibits multiple antiviral pathways, leading also to cell damage. PKR activation is known to promote apoptosis, and its dysregulation causes neurological disorders (26,63). Thus, it will be relevant in future studies to investigate the impact of sfRNA-mediated PKR activation on ZIKV pathogenesis.

Understanding how viruses co-opt fundamental cellular processes such as transcription, splicing and translation, to favor viral replication remains an active field of research, despite extensive research efforts. In this regard, we have previously shown that DENV NS5 usurps basic components of the splicing machinery, leading to a more favorable environment for viral replication by modulating gene expression (30,64). Here, activation of PKR was shown to lead to downregulation of translation of ∼70% of the genes analyzed, yet translation efficiency of ISGs was significantly lower than control genes with similar expression levels. Why are the antiviral genes more susceptible to these global changes in splicing or translation? Although we do not yet have an answer to this, it is possible that the kinetics of induction of highly regulated defense proteins, which are induced during infection, are more susceptible to global interruption of gene expression, an Achilles heel in the host defense system that is leveraged by the virus.

In summary, this work provides a molecular understanding of sfRNA functions during ZIKV infection, shedding light on basic aspects of mosquito-borne flavivirus biology and revealing a novel viral mechanism for co-opting the host antiviral defense.

Data availability

The generated data have been deposited in GEO and can be accessed at https://www.ncbi.nlm.nih.gov/geo/query/acc.cgi?acc=GSE254254.

Supplementary data

Supplementary Data are available at NAR online.

Acknowledgements

Authors are thankful to the members of the Gamarnik lab and Tzachi Hagai for critical reading of the manuscript, Ana Fernandez-Sesma for comments and suggestions about the work, and Susan Weiss for providing the PKR-/- A549 cells. HMP, SOR and GCN were granted CONICET fellowships. This work was performed as part of thesis research for L.A.C., Graduate School of the Stowers Institute for Medical Research. H.M.P. received the PROLAB scholarship granted by the American Society for Biochemistry and Molecular Biology (ASBMB).

Author contributions: H.M.P., A.B. and A.V.G. conceptualized and designed the experiments. H.M.P., M.M.G.L.L., S.O.R., L.A.C., G.S.C.N., A.J.F.A. and M.J.D. performed the experiments. H.M.P., D.V.A., D.E.A., A.B. and A.V.G. performed data processing and analysis. All authors contributed to the writing and editing of the paper.

Funding

NIH (NIAID) [U19AI168631-01]; Fondo Nacional para la Investigación Científica y Tecnológica [PICT 2019-02869]; CIHR-IRSC-ISF [495147 to A.V.G.]; NIH [1R01GM136849-01, 1R21OD034161-01]; Stowers Institute for Medical Research to A.B.; A.V.G., M.M.G.L.L., D.E.A. and A.F.A. are members of the Argentinean Council of Investigation (CONICET). Funding for open access charge: CIHR-IRSC-ISF [495147 to A.V.G.].

Conflict of interest statement

None declared.

References

1. Villordo,S.M., Carballeda,J.M., Filomatori,C.V. and Gamarnik,A.V. (2016) RNA structure duplications and flavivirus host adaptation. *Trends Microbiol.*, **24**, 270–283.
2. Göertz,G.P., Abbo,S.R., Fros,J.J. and Pijlman,G.P. (2018) Functional RNA during Zika virus infection. *Virus Res.*, **254**, 41–53.
3. Slonchak,A. and Khromykh,A.A. (2018) Subgenomic flaviviral RNAs: what do we know after the first decade of research. *Antiviral Res.*, **159**, 13–25.
4. Liu,Y., Liu,H., Zou,J., Zhang,B. and Yuan,Z. (2014) Dengue virus subgenomic RNA induces apoptosis through the bcl-2-mediated PI3k/akt signaling pathway. *Virology*, **448**, 15–25.
5. Donald,C.L., Brennan,B., Cumberworth,S.L., Rezelj,V.V., Clark,J.J., Cordeiro,M.T., Freitas de Oliveira França,R., Pena,L.J., Wilkie,G.S., Da Silva Filipe,A., *et al.* (2016) Full genome sequence and sfRNA interferon antagonist activity of Zika virus from Recife, Brazil. *PLoS Negl. Trop. Dis.*, **10**, e0005048.
6. Schuessler,A., Funk,A., Lazear,H.M., Cooper,D.A., Torres,S., Daffis,S., Jha,B.K., Kumagai,Y., Takeuchi,O., Hertzog,P., *et al.* (2012) West Nile virus noncoding subgenomic RNA contributes to viral evasion of the type I interferon-mediated antiviral response. *J. Virol.*, **86**, 5708–5718.
7. Zhang,Q.-Y., Li,X.-F., Niu,X., Li,N., Wang,H.-J., Deng,C.-L., Ye,H.-Q., Huang,X.-Y., Chen,Q., Xu,Y.-P., *et al.* (2020) Short direct repeats in the 3' untranslated region are involved in subgenomic flaviviral RNA production. *J. Virol.*, **94**, e01175-19.
8. Pijlman,G.P., Funk,A., Kondratieva,N., Leung,J., Torres,S., van der Aa,L., Liu,W.J., Palmenberg,A.C., Shi,P.Y., Hall,R.A., *et al.* (2008) A highly structured, nuclease-resistant, noncoding RNA produced by flaviviruses is required for pathogenicity. *Cell Host Microbe*, **4**, 579–591.
9. Akiyama,B.M., Laurence,H.M., Massey,A.R., Costantino,D.A., Xie,X., Yang,Y., Shi,P.Y., Nix,J.C., Beckham,J.D. and Kieft,J.S. (2016) Zika virus produces noncoding RNAs using a multi-pseudoknot structure that confounds a cellular exonuclease. *Science*, **354**, 1148–1152.
10. Pallarés,H.M., Navarro,G.S.C., Villordo,S.M., Merwaiss,F., Borba,L.d., Ledesma,M.M.G.L., Ojeda,D.S., Henrion-Lacritick,A., Morales,M.A., Fabri,C., *et al.* (2020) Zika Virus subgenomic flavivirus RNA generation requires cooperativity between duplicated RNA structures that are essential for productive infection in Human cells. *J. Virol.*, **94**, 343–363.
11. Slonchak,A., Wang,X., Aguado,J., Sng,J.D.J., Chaggar,H., Freney,M.E., Yan,K., Torres,F.J., Amarilla,A.A., Balea,R., *et al.* (2022) Zika virus noncoding RNA cooperates with the viral protein NS5 to inhibit STAT1 phosphorylation and facilitate viral pathogenesis. *Sci. Adv.*, **8**, eadd8095.
12. Filomatori,C.V., Carballeda,J.M., Villordo,S.M., Aguirre,S., Pallarés,H.M., Maestre,A.M., Sánchez-Vargas,I., Blair,C.D., Fabri,C., Morales,M.A., *et al.* (2017) Dengue virus genomic variation associated with mosquito adaptation defines the pattern of viral non-coding RNAs and fitness in human cells. *PLoS Pathog.*, **13**, e1006265.
13. Jones,R.A., Steckelberg,A.L., Vicens,Q., Szucs,M.J., Akiyama,B.M. and Kieft,J.S. (2021) Different tertiary interactions create the same important 3D features in a distinct flavivirus xrRNA. *RNA*, **27**, 54–65.
14. Szucs,M.J., Nichols,P.J., Jones,R.A., Vicens,Q. and Kieft,J.S. (2020) A new subclass of exoribonuclease-resistant RNA found in multiple genera of Flaviviridae. *Mbio*, **11**, e02352-20.
15. Graham,M.E., Merrick,C., Akiyama,B.M., Szucs,M.J., Leach,S., Kieft,J.S. and Beckham,J.D. (2023) Zika virus dumbbell-1 structure is critical for sfRNA presence and cytopathic effect during infection. *Mbio*, **14**, e0110823.
16. Sparks,H., Monogue,B., Akiyama,B., Kieft,J. and David Beckham,J. (2020) Disruption of Zika virus xrRNA1-dependent sfRNA1 production results in tissue-specific attenuated viral replication. *Viruses*, **12**, 1177 .
17. Pompon,J., Manuel,M., Ng,G.K., Wong,B., Shan,C., Manokaran,G., Soto-Acosta,R., Bradrick,S.S., Ooi,E.E., Missé,D., *et al.* (2017) Dengue subgenomic flaviviral RNA disrupts immunity in mosquito salivary glands to increase virus transmission. *PLoS Pathog.*, **13**, e1006535.
18. Bidet,K., Dadlani,D. and Garcia-Blanco,M.A. (2014) G3BP1, G3BP2 and CAPRIN1 are required for translation of interferon stimulated mRNAs and are targeted by a dengue virus non-coding RNA. *PLoS Pathog.*, **10**, e1004242.
19. Schnettler,E., Sterken,M.G., Leung,J.Y., Metz,S.W., Geertsema,C., Goldbach,R.W., Vlak,J.M., Kohl,A., Khromykh,A.A. and Pijlman,G.P. (2012) Noncoding flavivirus RNA displays RNA interference suppressor activity in insect and mammalian cells. *J. Virol.*, **86**, 13486–13500.
20. Göertz,G.P., Fros,J.J., Miesen,P., Vogels,C.B.F., van der Bent,M.L., Geertsema,C., Koenraadt,C.J.M., van Rij,R.P., van Oers,M.M. and Pijlman,G.P. (2016) Noncoding subgenomic flavivirus RNA is processed by the Mosquito RNA interference machinery and determines West Nile Virus transmission by Culex pipiens mosquitoes. *J. Virol.*, **90**, 10145–10159.

21. Soto-Acosta,R., Xie,X., Shan,C., Baker,C.K., Shi,P.Y., Rossi,S.L., Garcia-Blanco,M.A. and Bradrick,S. (2018) Fragile X mental retardation protein is a Zika virus restriction factor that is antagonized by subgenomic flaviviral RNA. *Elife*, **7**, e39023.
22. Moon,S.L., Anderson,J.R., Kumagai,Y., Wilusz,C.J., Akira,S., Khromykh,A.A. and Wilusz,J. (2012) A noncoding RNA produced by arthropod-borne flaviviruses inhibits the cellular exoribonuclease XRN1 and alters host mRNA stability. *RNA*, **18**, 2029–2040.
23. Michalski,D., Gustavo Ontiveros,J., Russo,J., Charley,P.A., Anderson,J.R., Heck,A.M., Geiss,B.J. and Wilusz,J. (2019) Zika virus noncoding sfRNAs sequester multiple host-derived RNA-binding proteins and modulate mRNA decay and splicing during infection. *J. Biol. Chem.*, **294**, 16282–16296.
24. Manokaran,G., Finol,E., Wang,C., Gunaratne,J., Bahl,J., Ong,E.Z., Tan,H.C., Sessions,O.M., Ward,A.M., Gubler,D.J., *et al.* (2015) Dengue subgenomic RNA binds TRIM25 to inhibit interferon expression for epidemiological fitness. *Science*, **350**, 217–221.
25. Lemaire,P.A., Anderson,E., Lary,J. and Cole,J.L. (2008) Mechanism of PKR activation by dsRNA. *J. Mol. Biol.*, **381**, 351–360.
26. Gal-Ben-Ari,S., Barrera,I., Ehrlich,M. and Rosenblum,K. (2019) PKR: a kinase to remember. *Front. Mol. Neurosci.*, **11**, 480.
27. Bonica,M.B., Goenaga,S., Martin,M.L., Feroci,M., Luppo,V., Muttis,E., Fabbri,C., Morales,M.A., Enria,D., Micieli,M.V., *et al.* (2019) Vector competence of Aedes aegypti for different strains of zika virus in Argentina. *PLoS Negl. Trop. Dis.*, **13**, e0007433.
28. Roche,R.R., Alvarez,M., Guzmán,M.G., Morier,L. and Kourí,G. (2000) Comparison of rapid centrifugation assay with conventional tissue culture method for isolation of dengue 2 virus in C6/36-HT cells. *J. Clin. Microbiol.*, **38**, 3508–3510.
29. Li,Y., Banerjee,S., Goldstein,S.A., Dong,B., Gaughan,C., Rath,S., Donovan,J., Korennykh,A., Silverman,R.H. and Weiss,S.R. (2017) Ribonuclease L mediates the cell-lethal phenotype of double-stranded RNA editing enzyme ADAR1 deficiency in a human cell line. *Elife*, **6**, e25687.
30. De Maio,F.A., Risso,G., Iglesias,N.G., Shah,P., Pozzi,B., Gebhard,L.G., Mammi,P., Mancini,E., Yanovsky,M.J., Andino,R., *et al.* (2016) The Dengue Virus NS5 protein intrudes in the cellular spliceosome and modulates splicing. *PLoS Pathog.*, **12**, e1005841.
31. Bazzini,A.A., Lee,M.T. and Giraldez,A.J. (2012) Ribosome profiling shows that miR-430 reduces translation before causing mRNA decay in zebrafish. *Science*, **336**, 233–237.
32. Ricciardi-Jorge,T., Lummertz da Rocha,E., Gonzalez-Kozlova,E., Rodrigues-Luiz,F., Ferguson,B.J., Sweeney,T., Irigoyen,N. and Santos Mansur,D. (2023) PKR-mediated stress response enhances dengue and Zika virus replication. *Mbio*, **14**, e0093423.
33. Ambrose,R.L. and Mackenzie,J.M. (2011) West Nile virus differentially modulates the unfolded protein response to facilitate replication and immune evasion. *J. Virol.*, **85**, 2723–2732.
34. Wang,Q., Xin,X., Wang,T., Wan,J., Ou,Y., Yang,Z., Yu,Q., Zhu,L., Guo,Y., Wu,Y., *et al.* (2019) Japanese encephalitis virus induces apoptosis and encephalitis by activating the PERK pathway. *J. Virol.*, **93**, e00887-19.
35. Gladwyn-Ng,I., Cordón-Barris,L., Alfano,C., Creppe,C., Couderc,T., Morelli,G., Thelen,N., America,M., Bessières,B., Encha-Razavi,F., *et al.* (2018) Stress-induced unfolded protein response contributes to Zika virus-associated microcephaly. *Nat. Neurosci.*, **21**, 63–73.
36. Protter,D.S.W. and Parker,R. (2016) Principles and properties of stress granules. *Trends Cell Biol.*, **26**, 668.
37. Campos-Melo,D., Hawley,Z.C.E., Droppelmann,C.A. and Strong,M.J. (2021) The integral role of RNA in stress granule formation and function. *Front. Cell Dev. Biol.*, **9**, 621779.
38. Rehwinkel,J. and Gack,M.U. (2020) RIG-I-like receptors: their regulation and roles in RNA sensing. *Nat. Rev. Immunol.*, **20**, 537–551.
39. Moreno,J.A., Radford,H., Peretti,D., Steinert,J.R., Verity,N., Martin,M.G., Halliday,M., Morgan,J., Dinsdale,D., Ortori,C.A., *et al.* (2012) Sustained translational repression by eIF2α-P mediates prion neurodegeneration. *Nature*, **485**, 507–511.
40. Sidrauski,C., Acosta-Alvear,D., Khoutorsky,A., Vedantham,P., Hearn,B.R., Li,H., Gamache,K., Gallagher,C.M., Ang,K.K.-H., Wilson,C., *et al.* (2013) Pharmacological brake-release of mRNA translation enhances cognitive memory. *Elife*, **2**, e00498.
41. Rabouw,H.H., Langereis,M.A., Anand,A.A., Visser,L.J., de Groot,R.J., Walter,P. and van Kuppeveld,F.J.M. (2019) Small molecule ISRIB suppresses the integrated stress response within a defined window of activation. *Proc. Natl. Acad. Sci. U.S.A.*, **116**, 2097–2102.
42. Metz,P., Reuter,A., Bender,S. and Bartenschlager,R. (2013) Interferon-stimulated genes and their role in controlling hepatitis C virus. *J. Hepatol.*, **59**, 1331–1341.
43. Schneider,W.M., Chevillotte,M.D. and Rice,C.M. (2014) Interferon-stimulated genes: a complex web of host defenses. *Annu. Rev. Immunol.*, **32**, 513.
44. Schoggins,J.W. (2019) Interferon-stimulated genes: what do they all do? *Annu. Rev. Virol.*, **6**, 567–584.
45. Pakos-Zebrucka,K., Koryga,I., Mnich,K., Ljujic,M., Samali,A. and Gorman,A.M. (2016) The integrated stress response. *EMBO Rep.*, **17**, 1374–1395.
46. Nishikiori,M., Den Boon,J.A., Unchwaniwala,N. and Ahlquist,P. (2022) Crowning touches in positive-strand RNA virus genome replication complex structure and function. *Annu. Rev. Virol.*, **9**, 193–212.
47. Cesaro,T. and Michiels,T. (2021) Inhibition of PKR by viruses. *Front. Microbiol.*, **12**, 757238.
48. Tu,Y.-C., Yu,C.-Y., Liang,J.-J., Lin,E., Liao,C.-L. and Lin,Y.-L. (2012) Blocking double-stranded RNA-activated protein kinase PKR by japanese Encephalitis virus nonstructural protein 2A. *J. Virol.*, **86**, 10347–10358.
49. Mudhasani,R., Tran,J.P., Retterer,C., Kota,K.P., Whitehouse,C.A. and Bavari,S. (2016) Protein kinase R degradation is essential for Rift Valley Fever virus infection and is regulated by SKP1-CUL1-F-box (SCF)FBXW11-NSs E3 ligase. *PLoS Pathog.*, **12**, e1005437.
50. Welsch,S., Miller,S., Romero-Brey,I., Merz,A., Bleck,C.K.E., Walther,P., Fuller,S.D., Antony,C., Krijnse-Locker,J. and Bartenschlager,R. (2009) Composition and three-dimensional architecture of the dengue virus replication and assembly sites. *Cell Host Microbe*, **5**, 365–375.
51. Whelan,J.N., Parenti,N.A., Hatterschide,J., Renner,D.M., Li,Y., Reyes,H.M., Dong,B., Perez,E.R., Silverman,R.H. and Weiss,S.R. (2021) Zika virus employs the host antiviral RNase L protein to support replication factory assembly. *Proc. Natl. Acad. Sci. U.S.A.*, **118**, e2101713118.
52. Ponia,S.S., Robertson,S.J., Mcnally,K.L., Bosio,C.M., Martens,C., Best,S.M., Subramanian,G., Sturdevant,G.L., Lewis,M., Jessop,F., *et al.* (2021) Mitophagy antagonism by ZIKV reveals Ajuba as a regulator of PINK1 signaling, PKR-dependent inflammation, and viral invasion of tissues. *Cell Rep.*, **37**, 109888.
53. Arnaud,N., Dabo,S., Maillard,P., Budkowska,A., Kalliampakou,K.I., Mavromara,P., Garcin,D., Hugon,J., Gatignol,A., Akazawa,D., *et al.* (2010) Hepatitis C virus controls interferon production through PKR activation. *PLoS One*, **5**, e10575.
54. Song,Y., Mugavero,J.A., Stauft,C.B. and Wimmer,E. (2019) Dengue and zika virus 5' untranslated regions harbor internal ribosomal entry site functions. *Mbio*, **10**, e00459-19.
55. Lefèvre,C., Cook,G.M., Dinan,A.M., Torii,S., Stewart,H., Gibbons,G., Nicholson,A.S., Echavarría-Consuegra,L., Meredith,L.W., Lulla,V., *et al.* (2023) Zika viruses encode multiple upstream open reading frames in the 5′ viral region with a role in neurotropism. bioRxiv doi: https://doi.org/10.1101/112904, 20 April 2023, preprint: not peer reviewed.
56. Edgil,D., Polacek,C. and Harris,E. (2006) Dengue virus utilizes a novel strategy for translation initiation when cap-dependent translation is inhibited. *J. Virol.*, **80**, 2976–2986.

57. Hou,S., Kumar,A., Xu,Z., Airo,A.M., Stryapunina,I., Wong,C.P., Branton,W., Tchesnokov,E., Götte,M., Power,C., *et al.* (2017) Zika virus hijacks stress granule proteins and modulates the host stress response. *J. Virol.*, **91**, e00474-17.
58. Roth,H., Magg,V., Uch,F., Mutz,P., Klein,P., Haneke,K., Lohmann,V., Bartenschlager,R., Fackler,O.T., Locker,N., *et al.* (2017) Flavivirus infection uncouples translation suppression from cellular stress responses. *Mbio*, **8**, e02150-16.
59. Villordo,S.M., Carballeda,J.M., Filomatori,C.V. and Gamarnik,A.V. (2016) RNA Structure Duplications and Flavivirus Host Adaptation. *Trends Microbiol.*, **24**, 270–283.
60. Villordo,S.M., Filomatori,C.V., Sánchez-Vargas,I., Blair,C.D. and Gamarnik,A.V. (2015) Dengue virus RNA structure specialization facilitates host adaptation. *PLoS Pathog.*, **11**, e1004604.
61. Reineke,L.C., Kedersha,N., Langereis,M.A., van Kuppeveld,F.J.M. and Lloyd,R.E. (2015) Stress granules regulate double-stranded RNA-dependent protein kinase activation through a complex containing G3BP1 and Caprin1. *Mbio*, **6**, e02486.
62. Paget,M., Cadena,C., Ahmad,S., Wang,H.T., Jordan,T.X., Kim,E., Koo,B., Lyons,S.M., Ivanov,P., tenOever,B., *et al.* (2023) Stress granules are shock absorbers that prevent excessive innate immune responses to dsRNA. *Mol. Cell*, **83**, 1180–1196.
63. Ma,C.H., Wu,C.H., Jou,I.M., Tu,Y.K., Hung,C.H., Chou,W.C., Chang,Y.C., Hsieh,P.L. and Tsai,K.L. (2019) PKR promotes oxidative stress and apoptosis of Human articular chondrocytes by causing mitochondrial dysfunction through p38 MAPK activation-PKR activation causes apoptosis in Human chondrocytes. *Antioxidants (Basel)*, **8**, 370.
64. Pozzi,B., Bragado,L., Mammi,P., Torti,M.F., Gaioli,N., Gebhard,L.G., García Solá,M.E., Vaz-Drago,R., Iglesias,N.G., García,C.C., *et al.* (2020) Dengue virus targets RBM10 deregulating host cell splicing and innate immune response. *Nucleic Acids Res.*, **48**, 6824.

Received: January 18, 2024. **Revised:** May 8, 2024. **Editorial Decision:** May 29, 2024. **Accepted:** June 4, 2024